Arabian Journal of Geosciences (2021) 14: 128
https://doi.org/10.1007/s12517-020-06418-z

1ST CAJG 2018

The Djilouet granite suite (Djanet terrane, eastern Hoggar, Algeria): petrography, mineralogy, geochemistry, and relations with quartz-cassiterite-wolframite vein systems

Fatiha Oulebsir[1] · Mokrane Kesraoui[1] · Dalila Nemmour-Zekiri[2] · Christian Marignac[3]

Received: 10 November 2019 / Accepted: 25 December 2020 / Published online: 18 January 2021

Abstract

The Djilouet complex forms a cupola made up of leucocratic granites associated with Sn-W mineralization. It could represent the Hoggar's easternmost rare metal granite (RMG) comparatively to those of the Taourirt province in the central Hoggar. It is located in the Djanet terrane, 12 km NE of the town of the same name in the far east of the Tuareg shield in Algeria. The Djanet terrane is made of a thick low-grade (greenschist facies) sedimentary sequence which was intruded by several generations of granitic rocks. The subcircular Djilouet body is made of leucocratic granites with progressive mutual transitions. Most of the outcrop is occupied by a porphyritic coarse-grained biotite granite. A muscovite granite is found in the center of the cupola, whereas a garnet (almandine—spessartite) granite forms a discontinuous rim all around it. Black micas from the biotite granite are lithian annite ("protolithionite"). The white micas from the muscovite granite and the garnet granite are classified as Fe-Li muscovite. The muscovite granite and the garnet granite contain accessory minerals as rutile, xenotime, monazite, zircon, and minerals that may be members of the pyrochlore supergroup. All the facies are leucogranite with high SiO_2 content and high K_2O-Na_2O ratio. They are poor in calcium and in mafic components and have very low phosphorus content ($P_2O_5 \sim 0.1\%$). The peraluminous composition is low to mild ($1.08 < A/CNK > 1.46$). The evolved granites of the Djilouet suite are enriched in Th and U, but the tantalum and the niobium are not highly concentrated (Ta + Nb = 10.4–17.1). The total REE content is low (57–84 ppm), and the patterns are typically wing shaped with a strong negative Eu anomaly and a small tetrad effect. The Sn-W mineralization consists two systems of veins: large quartz veins with ferberite ($H/F \sim 0.8$) and quartz veinlets or stockworks with homogeneous cassiterite and minor wolframite ($H/F \sim 48$). The iso-content contours of tin and tungsten, as produced from a sampling covering the whole cupola, overlap very little. The differences which were noted throughout the study between the Taourirt granites and those of the Djilouet suite are to be related to the lithological nature of the crust rather than to a difference in the geodynamic environment.

Keywords Djanet · Eastern Hoggar · Djilouet cupola · Leucocratic granites · Sn-W mineralization · Muscovite granite · Garnet-bearing granite

This paper was selected from the 1st Conference of the Arabian Journal of Geosciences (CAJG), Tunisia 2018

Responsible Editor: François Roure

✉ Fatiha Oulebsir
fatiha.oulebsir@gmail.com; foulebsir@yahoo.fr;
fatiha.oulebsir@usthb.dz

Mokrane Kesraoui
mkesraoui@gmail.com

Dalila Nemmour-Zekiri
nemourd@yahoo.fr

Christian Marignac
christian.marignac@univ-lorraine.fr

[1] Laboratory of Metallogeny and Magmatism of Algeria, FSTGAT/USTHB, BP n° 32 El Alia, 16111 Algiers, Algeria

[2] Laboratory of Geodynamics, Geology of the Engineer and Planetology, FSTGAT/USTHB, Algiers, Algeria

[3] Laboratoire Géoressources, UMR-CNRS 7359, Ecole des mines de Nancy, Campus ARTEM, CS14234, 54042 Nancy Cedex, France

Introduction

With main resource and production in China, the tungsten is recognized a critical strategic metal for western economy (e.g., European Commission 2017), and this observation has prompted a renewal in research and production of this metal. The central Hoggar has been known for a long time to host tungsten deposits, which were not seriously worked due to the environmental constraints (lack of water). Prospection in the 1980s by the SONAREM revealed ~ 100 rare metal (Sn-W-Ta-Li-B) occurrences, of which only a dozen was found to be of potential economic interest at the time. The known endowment is rather low (23.5 kt W: Mining Journal 2009).

It may therefore be useful to reevaluate the tungsten potential in the Hoggar. In this connection, the present work was focused onto the poorly known tin-tungsten occurrences of the easternmost Hoggar terranes.

At present, most of the known deposits and showings are in the Tamanrasset area (central Hoggar), associated to Li-F-rich rare metal granites (RMG) (Bouabsa 1987; Chalal and Marignac 1997; Kesraoui 1990; Kesraoui et al. 2000; Nedjari et al. 2001; Kesraoui and Nedjari 2002; Marignac et al. 2016). Emplaced at c. 539–525 Ma (Cheilletz et al. 1992), they are clearly related to the late Pan-African Taourirt granite province (Azzouni-Sekkal et al. 2003) thought to record the latest deformation events of the Pan-African cycle (Azzouni-Sekkal et al. 2003).

The Djilouet tin-tungsten mineralization is located in the Djanet terrane, the easternmost terrane of the Tuareg Shield. This terrane was for a long time poorly known, but several recent works allow a better understanding of its evolution and its place in the history of the shield (Fezaa et al. 2006; Nemmour-Zekiri et al. 2006; Oulebsir and Kesraoui 2006; Oulebsir 2009; Fezaa 2010; Fezaa et al. 2010; Nemmour-Zekiri 2012; Nemmour-Zekiri and Mahdjoub 2012; Fezaa et al. 2013; Liégeois et al. 2013; Oulebsir et al. 2013; Lamri et al. 2016). It becomes therefore possible to better conceptualize the context of the Djilouet mineralization and make a comparison with the central Hoggar mineralized province, as a potential help for future prospection.

The present work is intended to be a contribution to this objective. It addresses the petrography and geochemistry of the Djilouet pluton which hosts the deposit and a preliminary description of the mineralization and concludes the similarity and differences with the central Hoggar.

Geological setting: the Djanet terrane

The Djanet terrane is the easternmost terrane of the Tuareg Shield, a Cenozoic dome exhuming a complex of Archean and Paleoproterozoic rocks, reworked during the Neoproterozoic Pan-African orogeny and unconformably overlain by flat lying Paleozoic sedimentary rocks (Fig. 1).

Place of the Djanet terrane in the Tuareg Shield

With two other terranes (Aouzegueur and Edembo terranes), the Djanet terrane is part of the eastern Tuareg Shield, separated from the other segments of the Tuareg Shield by the Raghane meridian megashear zone (Fig. 1). West from the Raghane structure, the western and central Tuareg Shield were structured from *c*. 760 to *c*. 580 Ma as a consequence of the Pan-African collision with the West African Craton of continental terranes shaped by the c. 2 Ga Eburnean orogeny and intervening oceanic- and arc-type terranes (Liégeois et al. 2013; and references therein). In particular, in the central Hoggar, the LATEA superterrane is a metacratonic unit (Liégeois et al. 2003), which was invaded by Pan-African granites at the end of the Pan-African events, including the late c. 540-c. 520 Ma Taourirt province (Azzouni-Sekkal et al. 2003) associated to rare metal granites (RMG) related Sn-W mineralization (Marignac et al. 2016; and references therein).

East of the Raghane shear zone are found three terranes, parts of the Saharan metacraton (Liégeois et al. 2013), separated from each other by NE-SW trending major shear zones, in contrast with the dominant N-S direction of the megashear zones which mark the structure of the western and central parts of the Tuareg Shield. From west to east are found the Aouzegueur, Edembo, and Djanet terranes (Fig. 1) (Fezaa et al. 2010; and references therein). The Neoproterozoic oceanic Aouzegueur terrane was eastwardly up thrusted (800–650 Ma), and the structures were sealed by granite plutons at c. 600 Ma. The Edembo terrane is characterized by high-grade (amphibolite-facies) metamorphism, with pervasive migmatitization. It is separated from the Djanet terrane by the N130°–140°E Tin Amali Shear Zone (TASZ), a syn-cinematic migmatitic structure. The Djanet terrane is considered representing the western margin of a concealed craton (Murzuq metacraton), presently buried below the Mesozoic sediments of the Murzuq basin (Fig. 1). Indentation of this craton during the Murzukian orogeny (575–555 Ma) was responsible for deformation, metamorphism, and granitization of the eastern part of the Tuareg Shield (Fezaa et al. 2010; Liégeois 2019).

The Djanet terrane (Fezaa et al. 2010)

The Djanet terrane is made of a thick low-grade (greenschist-facies) sedimentary sequence (Djanet Group), strongly contrasting with the nearby high-grade Edembo terrane, which was intruded by several generations of granitic rocks.

The thick Upper Proterozoic Djanet Group is made of clastic series (slates, quartzites, and conglomerates) interleaved with decimeter to meter sills of andesite and rhyolite.

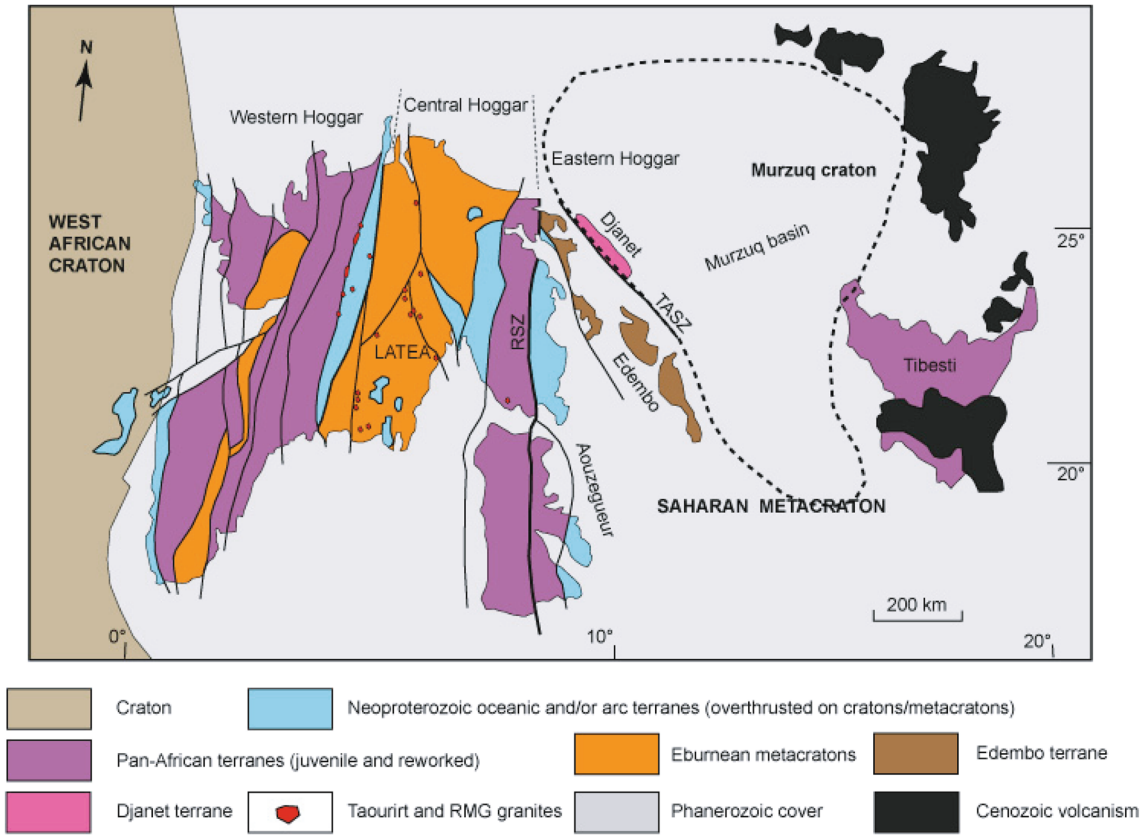

Fig. 1 The Hoggar Shield (adapted from Fezaa et al. 2010)

Detrital zircons from the Djanet Group were dated by LA-ICP-MS (Fezaa et al. 2013) yielding two age peaks, one Pan-African (younger than 635 Ma) and one Eburnean (c. 1.9 Ga). The youngest age of 589 ± 11 Ma constrains the age of the Group at 580 ± 10 Ma, taking into consideration the age of the oldest intrusion overprinting the metasediments. The Djanet Group sediments were weakly metamorphosed and deformed in the greenschist facies, with development of a slaty cleavage, at c. 570 Ma (Fezaa et al. 2010).

Several generations of Pan-African granite magmatism are known in the Djanet terrane and were dated by Fezaa et al. (2010) and Fezaa et al. (2010). The oldest is the large Djanet batholith constituted by a highly potassic calc-alkaline porphyritic amphibole-biotite-granite, dated at 571 ± 16 Ma, and coeval with migmatitization in the adjacent Edembo terrane (568 ± 4 Ma). It was followed by the intrusion of high-level circular plutons of coarse-grained syenogranite of the Tin Bedjane type, dated at 568 ± 5 Ma. A swarm of granodiorite to monzogranite dykes (Tin Amali Dyke Swarm) overprinted the preceding granites and was dated at 558 ± 5 Ma. This giant dyke swarm is slightly oblique to the NW-SE Tin Amali Shear Zone (TASZ) separating to the west Djanet and Edembo terranes (Lamri et al. 2016) and may therefore be interpreted as recording the shortening direction associated to the TASZ activity.

Place of the Djilouet massif in the Djanet terrane

The Djilouet area (Fig. 2) is an inlier of Upper Proterozoic rocks of the Djanet terrane, unconformably surrounded by the tabular Lower Paleozoic Tassili sedimentary formations (Ajjer series) (Fig. 3a, b). Rocks of the Djanet Group are dominant at the outcrop. To the exception of the Tin Bedjane syenogranites, all the granite generations are represented in the Djilouet area (Fig. 2). The Tin Amali dykes are here subparallel to the foliation of the Djanet Group. Three subcircular plutons (Edjéreou, Edjédjé, and Djilouet) (Fig. 3e) seem to have been the latest emplaced Pan-African plutons in the Djilouet area, but their precise age remains unknown. There are however NNW-SSE ductile shear zones in the vicinity of the Djilouet pluton that are clearly overprinted by the pluton (Fig. 4). There is no thermal metamorphism associated with the pluton emplacement, indicative of a shallow level of intrusion.

Brittle fracturing is well developed, with two main families, NW-SE (dextral) and NE-SW (Fig. 2), the latter controlling the Sn-W mineralization and displaying evidence of post-Paleozoic reactivation, as they may extend through the Tassili formations.

From the late Miocene to the early Quaternary, the area has been subjected to mafic volcanism, with flows and formation of cones of olivine basalt (Fig. 3h).

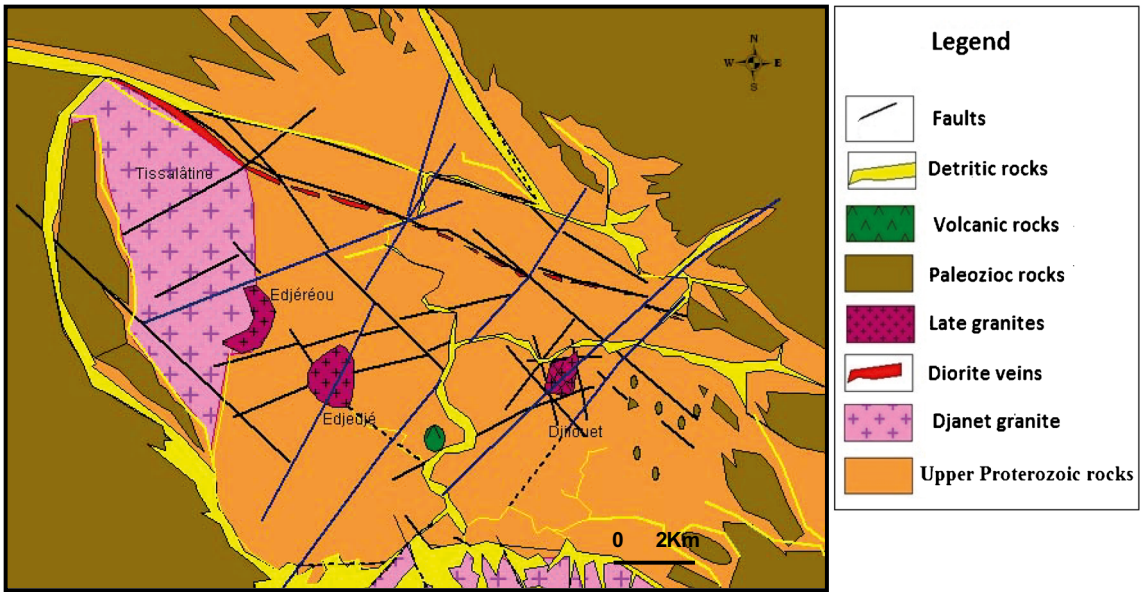

Fig. 2 Structural scheme of the Djilouet area from aerial photography (70 FG 32 III-IV/800 n° 194) (Oulebsir F, 2009)

The Djilouet pluton

The subcircular Djilouet body is made of five distinct granite types, displaying a concentric pattern (Fig. 4). Most of the outcrop is occupied by a porphyritic coarse-grained biotite granite. In the center of the body is found a muscovite granite, whereas a garnet-bearing granite forms a discontinuous rim all around the pluton. At the eastern border, the garnet-bearing granite gives way to a marginal smoked quartz granite. All these facies are overprinted by numerous thin aplite dykes (5–10 cm width) which may extend in the metasedimentary wall rocks. They display a more or less radial pattern and are mainly concentrated in the outer reaches of the pluton.

NE-SW elongated stripes of a greisen are present in the southwest half of the pluton, where they overprint all the facies, including the aplites (Fig. 4). Mineralized quartz veins (cassiterite and wolframite), with a similar orientation and greisenized borders, are distinctly separated from these greisen stripes, which they overprint.

Material and methods

A total of 50 samples from the different facies were studied for the petrography, of which 18 were selected for global analyses, BSE imaging, and EPMA/SEM-EDS microanalyses. Following petrographic examination with an OLYMPUS BX51 (transmitted and reflected light) optical microscope and a VHX-200 KEYENCE numeric microscope, selected samples were studied with a Schottky-FEG (Field Emission Gun) JEOL J7600F scanning electron microscope (SEM) equipped with an SDD-type EDS spectrometer at the GeoRessources Laboratory (Nancy, France). Backscattered electron (BSE) images were obtained by setting the acceleration voltage at 15 kV. Major element mineral compositions were determined in micas using a CAMECA SX100 Electron microprobe (EPMA) equipped with a wavelength dispersive spectrometer (WDS) and in accessory minerals using the same Schottky-FEG (Field Emission Gun) JEOL J7600F scanning electron microscope (SEM) equipped with a SDD-type EDS spectrometer, both at the GeoRessources Laboratory (Nancy, France). Analytical conditions were a 12 nA current and an accelerating voltage of 15 kV for the EPMA and a 1 nA current and an acceleration voltage of 15 kV for the SEM, with a counting time of 10 s. The same natural and synthetic oxides and silicate standards were used for the two types of analyses. For the micas, these standards were topaz (F), albite (Na), olivine (Mg), orthoclase (Si, K), wollastonite (Ca), $MnTiO_3$ (Ti, Mn), and hematite (Fe). For the accessories were added ZrO_2 (Zr), uraninite (U), thorianite (Th), arsenopyrite (As), La-monazite (La), Ce-monazite (P, Ce), Nd-monazite (Nd), REE-fluorides (other REE), $Y_3Fe_5O_{12}$ (Y), $SrSO_4$ (S), cassiterite (Sn), scheelite (W), and elemental Hf, Nb, Sc, and Ta.

Most of the bulk rock analyses were performed at the ORGM-Laboratory (Boumerdes, Algeria). Only three samples could be completely analyzed (major and trace elements) at the SARM l-Laboratory at the CRPG-Nancy. The samples were crushed and powdered in an agate mortar. They were prepared by fusion with a $LiBO_2$ and HNO_3 dissolution. Major elements were analyzed by ICP-OES, while trace elements (including REE) have been obtained by ICP-MS.

Powder X-ray diffraction was used for the characterization of wolframite at the ORGM-laboratory (Algeria). The sample preparation consists in separating the different mineral phases and then reducing them to a very fine powder (< 40 μm) using an agate mortar. The powder is then placed on a sample holder

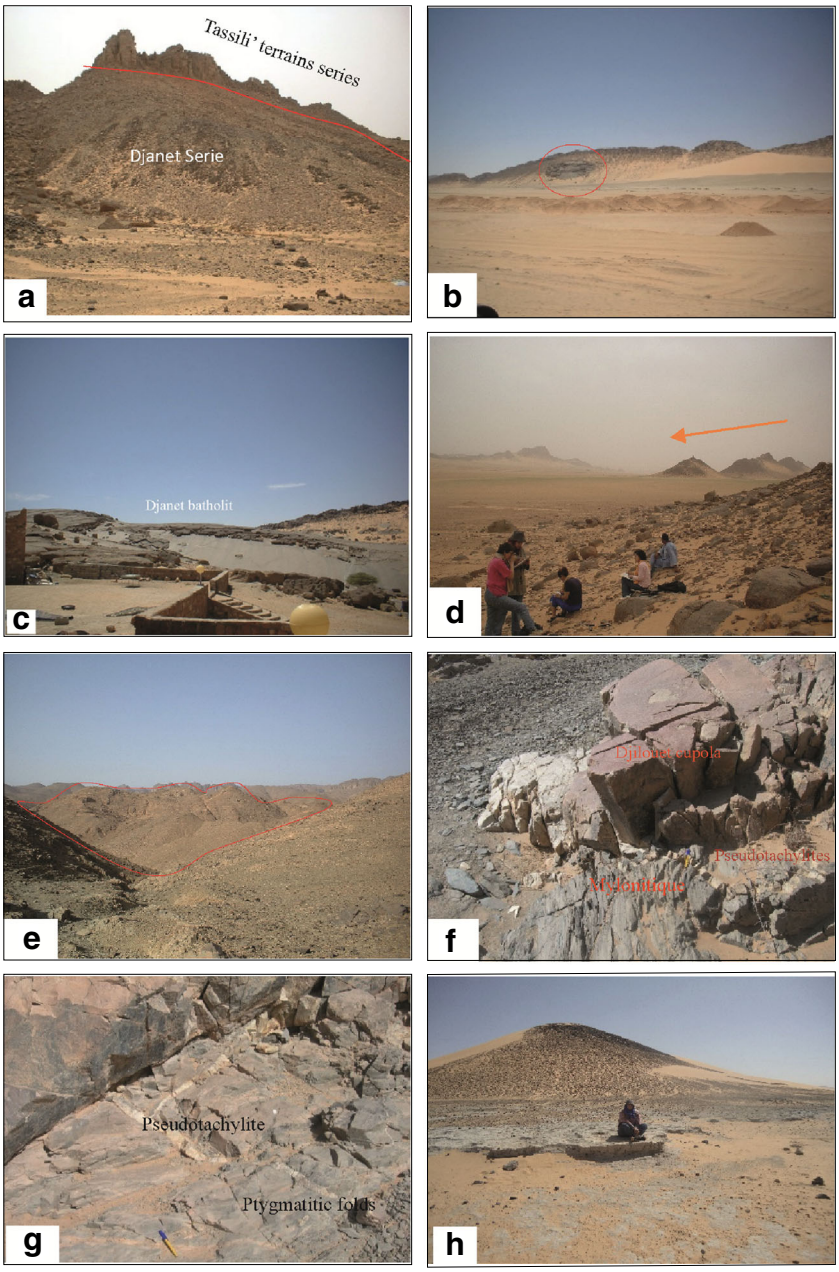

Fig. 3 Field views. (**a**) The Djanet group: Djanet series and deposits of the Tassili' terrains, series separated by a major unconformity. (**b**) Large porphyroid Djanet batholiths type intersecting the Djanet group. (**c**) Large porphyroid Djanet batholiths. (**d**) Tin-Amali dykes-oriented SE-NW. (**e**) latest pluton's leucocratic granite of Djilouet type. (**f**) Mylonitic rocks and pseudotachylites bordering on SW Djilouet cupola. (**g**) The granitoid with ptygmatitic folds and pseudotachylites in shales. (**h**) Basaltic cone

so as to create a carefully flat surface. Once the sample was subjected to X-ray diffraction analysis, their respictive diffractograms will be recorded using a Philips high-voltage generator equipped with a copper anode with a wavelength of 1.5405 Å. The diffractograms were recorded using a Philips high-voltage generator equipped with a copper anode with a wavelength of 1.5405 Å. The samples are scanned step by step. The instrument is equipped with software called "diffrac plus release 2005" to facilitate the reading of the diffractograms. The scanning starts at 5° (2°θ) and ends at 70° (2°θ). The generator produces a current of 50 m A and a voltage of 40 kV.

Petrography

Biotite leucogranite

The pinkish gray biotite granite (Fig. 5a) is a porphyritic leucogranite with quartz, K-feldspar, plagioclase, and biotite macrocrysts set in a fine-grained (0.3 to 0.5 mm) matrix of quartz, microcline, plagioclase, and rare biotite (Fig. 5b). It contains rounded mafic enclaves (4–5 cm). It is a two micas granite, in which however muscovite is clearly a subsolidus phase (see below). Perthitic K-feldspar macrocrysts (up to 1 cm) are less abundant than the plagioclase macrocrysts.

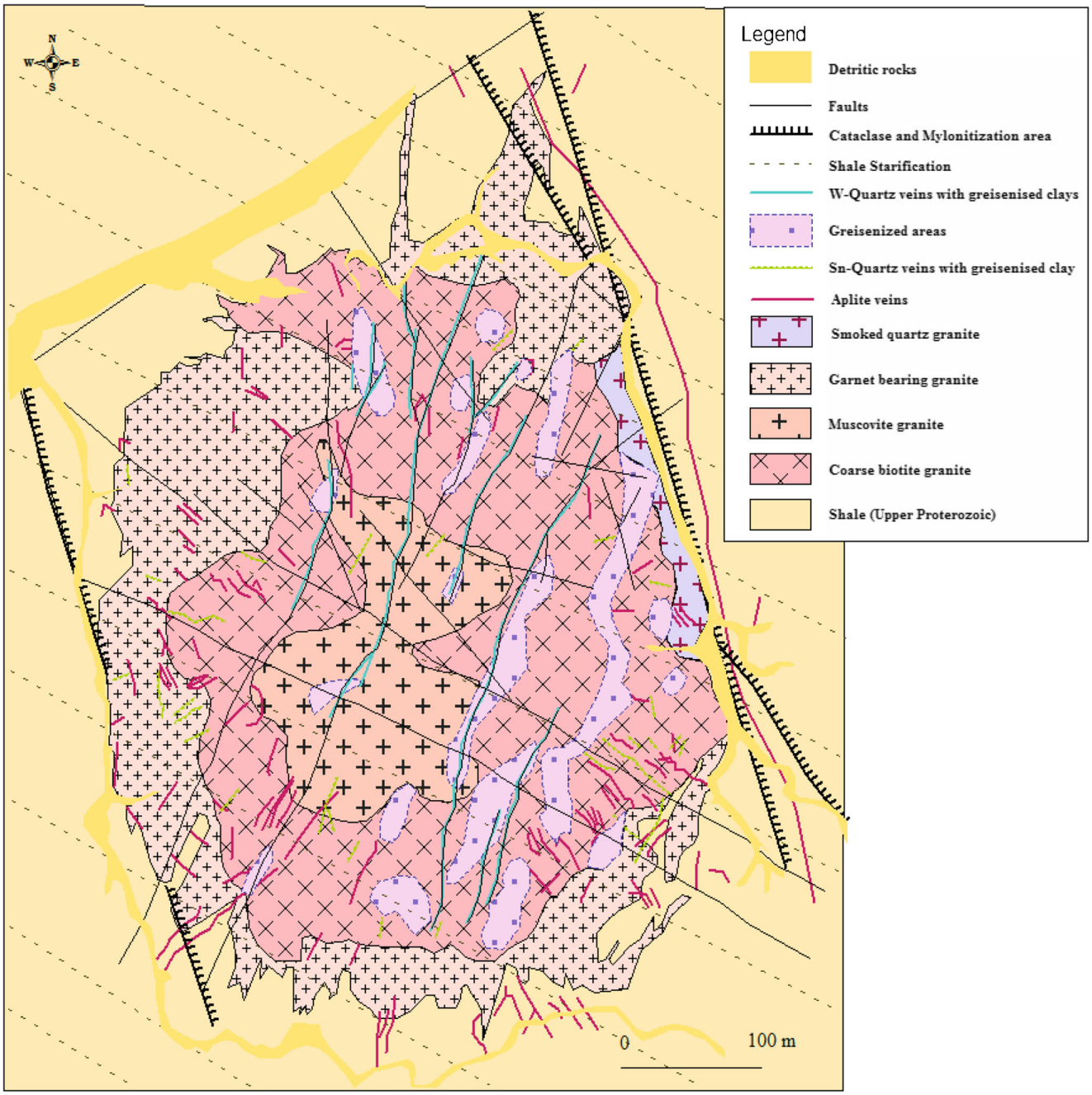

Fig. 4 Geological map of the Djilouet pluton, redrawn and modified (based on a SONAREM report for 1986)

The latter forms euhedral to subhedral plagioclase crystals, with two populations, one of large (up to 1 cm) crystals and another of smaller crystals (3–5 mm), which may be included in the K-feldspar macrocrysts. Quartz (3–5 mm) and biotite (4–5 mm) macrocrysts are of the same size as this second population. Biotite is very subordinated, with variable abundance (≤ 15 vol%). Smaller biotite crystals (100–200 μm) are locally scattered in the K-feldspar macrocrysts. In the matrix, K-feldspar (commonly microcline) is more abundant than the plagioclase. Quartz macrocrysts may locally be very abundant. They are subhedral, typically with thin aureoles of intergrown quartz and microcline (micropegmatite) (Fig. 5d, 6d), whereas in the matrix, quartz is present both as rounded granules and interstitial anhedral patches. The plagioclase is zoned, with an oligoclase (An25–27) core, without apparent compositional zoning, separated by a break from a more albitic rim, up to 200 μm in width (Fig. 5c). This rim is however absent from the microphenocrysts (An35) included in the K-feldspar. K-feldspar is a nearly pure orthoclase (K/K + Na between 0.89 and 0.99, average 0.95), while the perthite is nearly pure albite (An05–07). Biotite is an Mg-lithian annite (see below, "Mineralogy"). Among the accessory minerals,

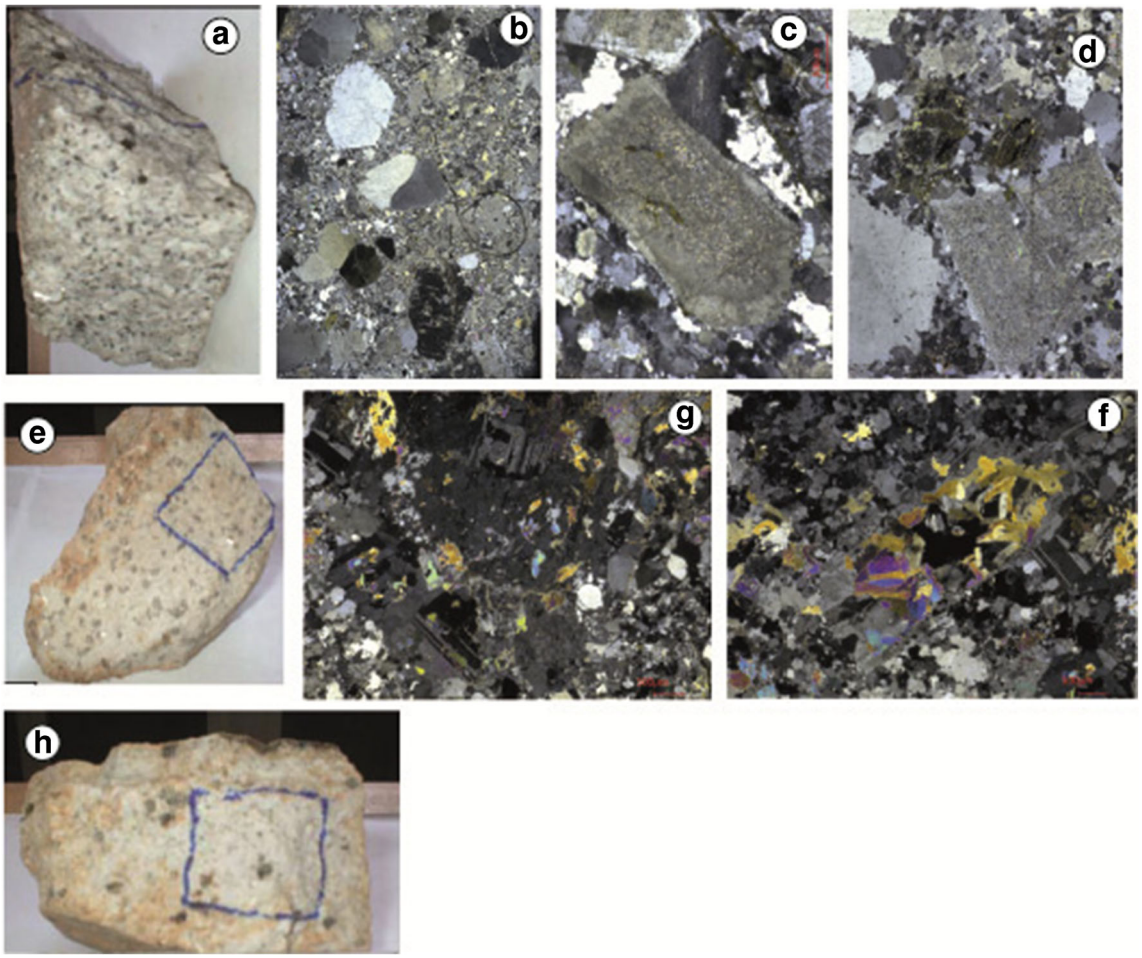

Fig. 5 Petrography of the Djilouet suite. **a**–**d** Biotite granite. **a** Macroscopic appearance (sample Fdj 2). **b** Microscopic appearance (plane polarized light [PPL], sample Fdj-2′). **c** Zoned plagioclase; note the sericite alteration restricted to the core. **d** PPL, sample Fdj-2. **e**–**g** Muscovite granite. **e** Macroscopic appearance (sample 19). **f** Aggregates of primary muscovite (PPL, sample Dj-21). **h** Garnet-bearing granite

zircon, apatite, ilmenite, monazite, titanite, and aeschynite may be considered primary (magmatic). Others are secondary minerals related to alteration processes (see below): rutile, epidote, fluorite, a fluoro-carbonate of REE, and uranothorianite. Zircon is abundant, most commonly found as small euhedral inclusions (≤ 50 μm) in the biotite. Hafnium content is moderate, comprised between 0.43 and 2.03 wt% HfO_2, without conspicuous zoning. Apatite is a fluor-apatite, commonly as small (≤ 50 μm) euhedral crystals accompanying the zircon in the biotite. Ilmenite is present either as large blocky prisms (100–150 μm) included in the biotite (Fig. 6b), or as tiny prisms included in the matrix in the close vicinity of biotite (Fig. 6e). It is a manganoan ilmenite, with an Mn/Fe + Mn ratio comprised between 0.15 and 0.40. Titanite is uncommon and associated to the large ilmenite. It is an F-titanite. A unique occurrence of probable aeschynite was observed as a nano-inclusion (0.2 μm) in quartz, close to ilmenite (Fig. 6e). Dispersed monazite crystals (20–100 μm) are included in muscovite (Fig. 6c). They are quite commonly rimmed by a fluor-apatite with micro-inclusions (1–2 μm) of uranothorianite to U-rich thorianite (Th/Th + U between 0.18 and 0.63), likely representing an alteration assemblage of the monazite (Fig. 6f). It is a Th-rich Ce-monazite (see below, "Mineralogy").

Mafic enclaves are fine-grained (100–150 μm), with a matrix of biotite-plagioclase, in equal proportion, dotted with millimetric ocelles of a plagioclase dominated-biotite assemblage (Fig. 6a). The ocelles are rimmed with biotite, and the enclave border is characterized by accumulation of biotite (up to 90 vol%) on 5 mm, whereas in close vicinity to this boundary, the abundance of small biotite laths in the granite is higher than elsewhere in the matrix. The plagioclase is sodic andesine (An33) in the ocelles, zoned with andesine core (An44–48) and oligoclase rim (An28) in the enclave. Biotite is lithian annite (see below, "Mineralogy").

Main alteration minerals are chlorite, muscovite, and a Mn-bearing calcite (2.2w% MnO). Chlorite resulted from biotite alteration, with conservation of the Fe/Fe + Mg ratio.

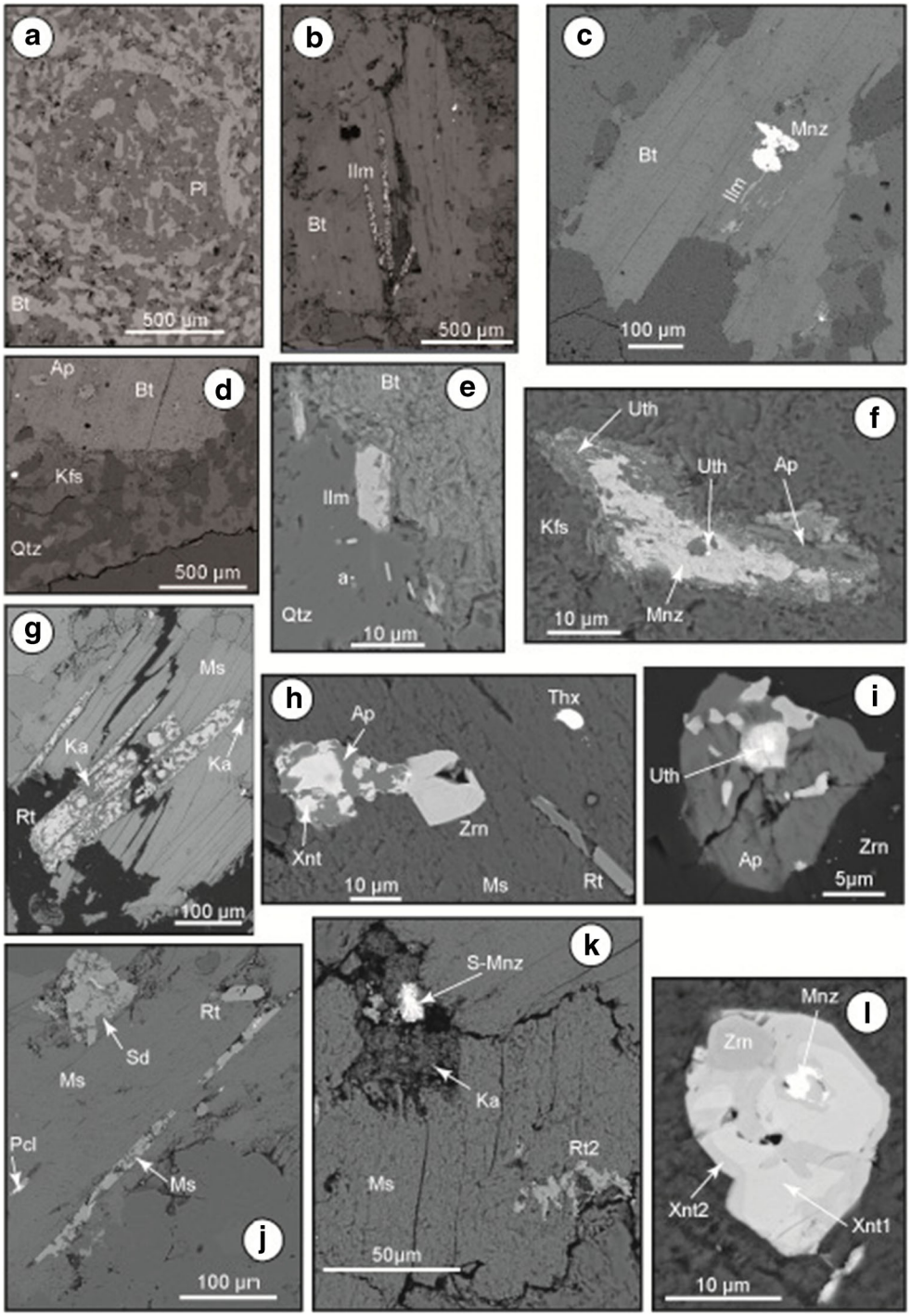

Muscovite either replaced biotite or was developed in feldspars, either as sericite alteration in the plagioclase cores or as muscovite flakes (Fig. 5c, d). It is a Fe-Li muscovite (see below, "Mineralogy"). Muscovite abundance is variable and clearly correlated to the distance to the greisenized strips affecting the Djilouet pluton: close to the greisens, practically all the biotite was replaced by muscovite. When replacing biotite, muscovite is associated to a rutile (30–50 µm) which is enriched in niobium (up to 2.37 wt% Nb_2O_5) and tungsten (up to 4.63 wt% WO_3) (Table 2). Fluorite, as small 3 mm euhedral crystals, is associated to the sericite in the altered plagioclase. In a unique occurrence, a fluoro-carbonate of calcium and LREE (Y-rich synchysite) was observed forming a felt of tiny filaments 5–10 µm along the mica cleavage. It was presumably formed concomitantly with fluorite. The Th-monazite is quite commonly rimmed by a fluor-apatite with micro-inclusions (1–2 µm) of either uranothorianite or an intimate association of xenotime-thorite solid solution with uranothorianite, likely representing an alteration assemblage. Monazite is occasionally observed as relicts rimmed by an

◀ **Fig. 6** Mineral assemblages in the Djilouet suite (BSE images). When no specified, all abbreviations are conformed to IMA recommendations (Whitney and Evans 2010). **a**–**f** biotite granite (sample Fdj-2′). **a** Detail of an ocelle in a MME enclave. **b** Ilmenite prisms (altered) included in biotite. **c** Ilmenite and monazite in biotite. **d** Micropegmatite at a magmatic quartz border; note the symplectic quartz-biotite association at the boundary of a biotite phenocryst. **e** Small euhedral ilmenite in quartz at the biotite border; **a** is an aeschynite nano-inclusion. **f** Monazite rimmed by apatite with uranothorianite nano-inclusions (Uth). **g**–**l** Muscovite granite. **g** Rutile 1 prisms in muscovite 1; the rutile is corroded by kaolinite (sample L13). **h** Primary xenotime-zircon assemblage and late F-apatite; note the faint zoning in the zircon; *Thx* thorite-xenotime solid solution (sample Dj-19). **i** Inclusions of zircon and uranothorianite (Uth) in a F-apatite (sample Dj-19). **j** Rutile 1 prisms in muscovite; the rutile is corroded, either by a muscovite or by siderite; note the development of an hydrated ferroan betafite (Pcl) overprinting the rutile (sample Dj-19). **k** Secondary rutile 2 and a S-rich monazite (S-Mnz) included in muscovite (sample L13). **l** Complex association of zircon, monazite, and two generations of xenotime, included in muscovite (sample Dj-19) (suite). **m**–**r** Garnet granite (sample Dj-14b). **m** Altered rutile 1 (corrosion by kaolinite) in muscovite; note the hydrated betafite (Pcl) insinuated in the cleavage and overprinting the rutile. **n** Detail, showing the betafite (Pcl) overprinting kaolinite. **o** Complex association of zircon, monazite, and xenotime, the latter corroding the earlier zircon-monazite assemblage. **q** Aggregates of fibrous monazite associated to scorodite (Scr). **r** Laths of a arsenopyrite transformed intoscorodite and replace by a complex arsenate solid solution of gasparite and chernovite (Gsc). **s** Smoked quartz granite (sample Dj-15): dissolution cavity at the expense of arsenopyrite, successively filled by scorodite (Scr) and a Ba-rich pharmacosiderite (Pcs)

epidote of the allanite group, likely representing another alteration assemblage.

Muscovite granite

The white muscovite granite (Fig. 5e) is a porphyritic leucogranite, with quartz, K-feldspar, muscovite, and albite macrocrysts set in a fine-grained matrix of quartz-albite-K-feldspar (0.2–0.3 mm) and muscovite (0.05–0.3 mm). The macrocrysts display a heterogranular distribution, with decreasing size order perthitic K-feldspar (up to 1.5 cm), quartz (0.3 to 0.6 cm), albite (0.2–0.3 cm), and muscovite (0.5–1.8 mm). In addition, there is a population of microphenocrysts of quartz and albite (~ 0.5 mm) set in the matrix, with some of the latter being included in the K-feldspar. Quartz macro- and microphenocrysts, of variable habit (rounded to sub-euhedral), and commonly forming syneusis of two or three crystals, typically display a thin lace-shaped overgrowth. Quartz in the matrix is in the form of either rounded granules, or anhedral interstitial patches. Anhedral quartz, being slightly larger than the average crystal size in the matrix, gives to the latter a heterogranular appearance. K-feldspar is mainly microcline, in the matrix. It is a nearly pure orthoclase, with a K/K + Na ratio between 0.96 and 0.98. Albite macrocrysts, albite in the perthite and albite in

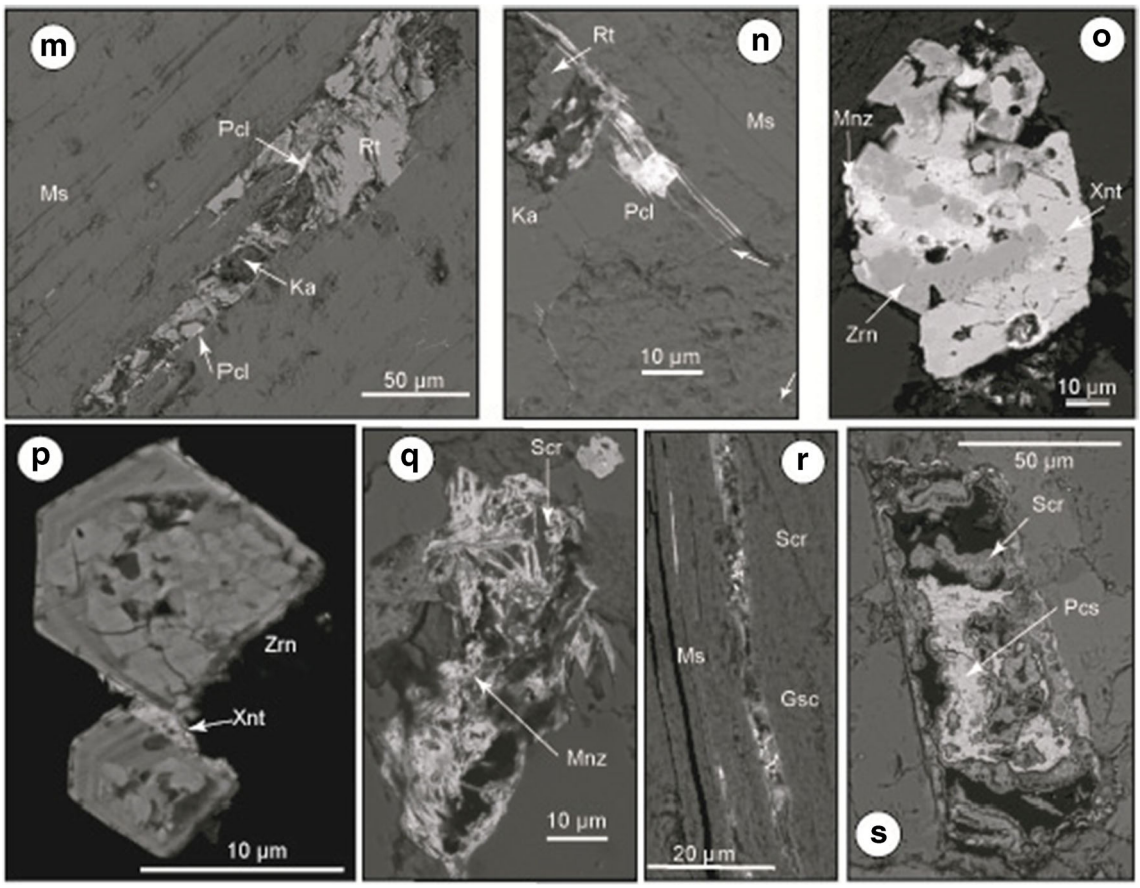

Fig. 6 (continued)

the matrix is nearly pure (An01 to An03). Muscovite is present either as large subhedral flakes, more or less aggregated (occasionally forming large, pluri-millimetric, more or less ellipsoidal, packages: Fig. 5f), or as irregular patches of smaller crystals overprinting the feldspars (Fig. 5g) and commonly associated to anhedral quartz. It is a Fe-Li muscovite (see below, "Mineralogy"). The large flakes commonly display a patchy zoning in BSE images, with darker gray parts developed along the cleavages or as irregular patches a few 10 μm in size. Occasionally, small biotite crystals are found, included in quartz.

Among the accessory minerals, rutile, zircon, monazite, apatite, xenotime, and uranothorite may be considered primary (magmatic). Others are secondary minerals: S-rich monazite, a fluoro-carbonate of REE, fluorite, and a Mg-Fe carbonate. Rutile is mainly found as elongated prismatic crystals along the muscovite cleavage, in the same way as ilmenite is found in the biotite of the biotite granite (Fig. 6g). It contains variable iron contents (0.61 to 3.29 wt% Fe) and variable contents of rare metals (0.46 to 1.16 wt% Nb, < 0.1 to 1.05 wt% Ta and 0.2 to 0.68 wt% W), with however Nb being commonly the more abundant (Table 2). A unique occurrence of a small (3 μm) pure ilmenite crystal included in the rutile equally contained more niobium (0.96% Nb_2O_5) than tungsten (0.33 wt% WO_3). Euhedral zoned (oscillatory zoning OZ) zircon crystals may be very small (from 1 μm to a few 10 μm). They are mainly included in muscovite and the feldspars. The hafnium content in the zircon is variable, from common moderate values (1.38–1.73 wt% HfO_2) up to 3.7–5.0 wt% HfO_2. Monazite is a Ce-monazite with a low Th content (see below, "Mineralogy"). A few small crystals (20–30 μm) of pure F-apatite were found, always containing micro-inclusions of ilmenite and zircons, the latter with uranothorite micro-inclusions (Fig. 6i). Xenotime is quite uncommon and only found in assemblages with other accessory minerals, for example, a primary assemblage of zircon, monazite, and xenotime 1, all being wrapped, and the phosphates corroded, by a xenotime 2 (Fig. 6l), or the association of uranothorite with a syneusis of zircon and xenotime 1, the latter wrapped and corroded by F-apatite (Fig. 6h). Xenotime 2 differs from xenotime 1 by a higher content in Y and a correlatively lesser content in HREE (see below, "Mineralogy"). Uranothorite is in fact a solid solution with xenotime (see below, "Mineralogy").

Alteration is mainly marked by the patchy zoning in muscovite, but a series of microassemblages of various secondary minerals are equally observed. Rutile typically displays a corroded appearance, with development of interconnected microcavities filled by either muscovite or, more commonly, kaolinite (the latter likely resulting of an alteration of the former), which may have expanded into the hosting muscovite (Fig. 6g). In one sample, a microvug was developed in the muscovite, filled with kaolinite and a radiating aggregate of small (5 μm) prisms of a S-rich monazite (see below, "Mineralogy") (Fig. 6k). Other S-rich monazites are found directly overprinting muscovite cleavage or as microcracks in the rutile (orthogonal to the prism axis). A secondary rutile is observed as microcracks affecting either muscovite, or albite or quartz (Fig. 6k). It is significantly enriched in tungsten relative to the primary rutile (2.1 wt% W) (Table 2). A late mineral of the pyrochlore supergroup (see below, "Mineralogy") may be observed having overprinted both rutile and the hosting muscovite, with preferential development as tiny rims for the rutile (Fig. 6j). A primary uranothorite (rich in Y: see below, "Mineralogy") was transformed into a fluoro-carbonate of REE (an Y-rich synchysite).

An Mg-Fe carbonate (Fe/Fe + Mg between0.6 and 0.9), which may be found corroding rutile (Fig. 6j), was a very late phase, as it post-dated a hydrothermal sulfide assemblage of pyrite and chalcopyrite, in association with fluorite. Likely coeval small euhedral (20 μm) fluorite crystals are found included in the albite.

Garnet-bearing granite

The garnet-bearing granite is a white porphyritic leucogranite, dotted with a red garnet (Fig. 5e) with perthitic microclinized K-feldspar (K/K + Na around 0.95). K-feldspar in the matrix is mainly represented by the microcline. Fine-grained matrix, quartz display heterogranular distribution as observed in muscovite granite. Abundance of fine-grained muscovite in the matrix, it is commonly associated with anhedral quartz, or in inclusion in feldspars. Albite in the matrix (100–200 μm) is zoned, with a pure albite rim (An00). Muscovite is a Fe-Li muscovite (see below). Garnet is abundant, displaying either a euhedral habit (100 μm) or forming contorted atolls included in the quartz. It is a Mn-rich almandine, with the average structural formula $(Ca_{0.03}Mg_{0.02}Fe^{2+}_{2.11}Mn_{0.74})Al_{2.05}(Si_{3.02}O_{12})$.

Among the accessory minerals, zircon, rutile, xenotime, and monazite may be considered primary (magmatic). Others are secondary minerals: mainly a member of the pyrochlore supergroup (see below, "Mineralogy"). Zircon occurs as small (5 to 30 μm) crystals, faintly zoned (OZ) and metamict. It contains a variable content in hafnium (2.18 to 5.33 wt% HfO_2), higher in average than in the muscovite granite. Rutile is found along the muscovite cleavage, just as in the muscovite granite. It may be rich in niobium (1.31 to 8.20 wt% Nb_2O_5), with minor tungsten (*bdl* to 1.02 wt% WO_3) and occasional scandium (0.58 Sc_2O_3) and tantalum (0.81 wt% Ta_2O_5) contents. Xenotime is common, found as small (5–30 μm) subhedral crystals included in K-feldspar, in muscovite, or at the interface between albite and muscovite. It may be intimately associated to zircon, either acting as cement for a zircon syneusis (Fig. 6p) or, in a unique

occurrence, overgrowing onto a primary assemblage of Th-monazite and zircon, both corroded by the xenotime (Fig. 6o). Xenotime composition is variable, comparable either to xenotime 1 or to xenotime 2 in the muscovite granite. Small (10–20 μm) euhedral Th-monazite is uncommon, always found close to the zircon; it is a Th-monazite (15.95 to 28.96 wt% ThO_2).

Alteration: Muscovite displays a patchy zoning, less conspicuous than in the muscovite granite, but with similar appearance. Rutile exhibits a corroded appearance, as in the muscovite granite. The granite contained arsenopyrite, as large euhedral crystals which were totally replaced by scorodite or even by iron hydroxides. In one occurrence, the (now transformed into scorodite) arsenopyrite seems to have been intimately associated, in a microvug at the muscovite-quartz interface, to a fibrous aggregate of a Th-monazite, less enriched in thorium (10.27 wt% ThO_2) than the primary monazite (Fig. 6q). Laths of arsenopyrite in the muscovite cleavage were transformed into scorodite and then overprinted by a complex arsenate solid solution between Y-chernovite and Nd-gasparite, with formula $Ca_{0.18}Y_{0.53}(Ce_{0.09}Nd_{0.17}Sm_{0.07}Gd_{0.10}Dy_{0.10})(Si_{0.08}P_{0.23}As0.78)(O_{3.58}F_{0.33})$ (Fig. 6r). Several other microassemblages are of secondary origin. Members of the pyrochlore supergroup are the most abundant. They display variable compositions (see below, "Mineralogy"). More common is a Ti-rich Y-poor phase, which may contain relicts of an Y-rich phase, and is mainly found overprinting the rutile and its hosting muscovite, rimming the rutile, or as microcracks in the muscovite or the feldspars (Fig. 6m, n).

Smoked quartz granite

This granite is characterized by the presence of smoked quartz, as either small megacrysts (2–5 mm) or veinlets. It is otherwise a garnet-bearing muscovite granite texturally similar to the garnet-bearing granite, except that the granulometry is slightly reduced: macrocrysts no more than 3 mm and fine-grained matrix in the 100–300 μm range, so that it may be considered a sub-type (a marginal facies) of the garnet-bearing granite. Two populations of muscovite (a Li-Fe muscovite: see below, "Mineralogy") are clearly expressed, mm-sized euhedral flakes and small anhedral patches, in the feldspars macrocrysts and in the matrix, where it is associated with anhedral interstitial quartz. Primary (magmatic) accessory minerals are zircon, apatite, rutile, and xenotime. Secondary minerals are mainly members of the pyrochlore supergroup (see below, "Mineralogy"). Rutile prisms along the muscovite cleavage is niobium-rich (0.96 to 2.93 wt% Nb_2O_5), with subordinate tantalum (*bdl* to 0.68 wt% Ta_2O_5) and tungsten (*bdl* to 0.58 wt% WO_3).

Alteration: As in garnet granite, large arsenopyrite crystals were completely dissolved and the cavity filled by a succession of scorodite and a Ba-pharmacosiderite with formula $(K_{0.14}Ca_{0.15}Ba_{0.54})$ $(Al_{0.4}Fe_{3.76})$ $(Si_{0.12}P_{0.43}As2_{.58})$ $O_4(OH)_5.5H_2O$ (Fig. 6-S). Primary rutile is partially replaced by pyrochlore 1, the latter being affected by microcracks of pyrochlore 2. Pyrochlore 2 differs from pyrochlore 1 by greater hydration, lower Nb, and higher Y contents.

Aplite

The aplite is a fine-grained sub-isogranular quartz-K-feldspar-albite rock (100 μm), with a few microphenocrysts (K-feldspar, albite) (50–100 μm) and additional muscovite. Quartz is interstitial. K-feldspar (locally, microcline) is subhedral, and larger crystals contain albite inclusions (50 μm). Albite is subhedral and presents the "Ala" twin. Muscovite is present as small irregularly distributed flakes looking secondary (30 μm). The only observed accessory mineral is zircon.

Greisens

The granites and the aplitic dykes of the Djilouet massif are subjected to intense metasomatic transformation under the effect of the circulation of hydrothermal fluids mineralizing at the stage of productive mineral genesis. These transformations are expressed by the establishment of greisen zones and greisenized granites with thicknesses of about 20–250 m and essentially NE direction. The primary rock textures in the greisenization zone are totally obscured. The greisen is a grayish (Fig. 5), medium-grained rock with a grained texture showing minerals in irregular patches. It consists essentially of quartz (25–35%) and white mica (50–55%). The greisen associated with the Quartz-cassiterite veinlets and stockworks is a white mica-quartz rock, with cassiterite and fluorite as accessory minerals, and disseminated relicts of K-feldspars (microcline). The white mica, by far the most abundant, is a Fe-Li muscovite (see below, "Mineralogy"). It forms conspicuous aggregates of millimetric euhedral crystals, locally bent or kinked. Quartz is subordinated and forms anhedral patches displaying undulating extinction. Cassiterite is abundant, present as small (500 μm) euhedral crystals with a typical dipyramid habit. Fluorite is less common and found either as subhedral plurimillimetric crystals embedded in the muscovite aggregates or small granules included in the micas.

Deformation

All facies display evidence of subsolidus plastic deformations, well expressed, in particular, in the marginal granites, but equally important in the central muscovite

granite. Magmatic quartz consistently shows waving extinction in all facies. Feldspars and muscovite were bent or even kinked, with in addition development of albitic cracks in the perthitic K-feldspars. In the muscovite- and garnet- bearing granite, the two generations of white micas may have been affected. It is possible, for example, to observe in a bent microcline a fissure of secondary muscovite, which was in turn kinked. The same style of deformation equally affected the greisen strips.

Mineralogy

Micas

Trioctahedral micas (lithian Mg-annite)

Black micas from the biotite granite and relicts (muscovitized biotite) from the muscovite granite were analyzed by EPMA (representative analyses in Table 1 and full data in Appendix

Table 1 Representative EPMA data for the micas of the Djilouet granites. The Li content was estimated in the trioctahedral micas from their silica content, according to $Li_2O^* = (0.287xSiO_2)-9.552$ (Tischendorf et al. 1999), and in the dioctahedral micas from their F content, according to the empirically adjusted equation: $L_{i2}O^* = 0.95 + 1.3F^{1.326}$ (see text for explanation)

	Trioctahedral			Dioctahedral							
	Biotite granite				Muscovite granite					Garnet-bearing granite		Greisen
					Ms1			Ms2		Ms1		
Sample	Fdj-1	Fdj-2	18 N	Dj-4	L19	Dj-21	Dj-21b	Dj-5	L13	Dj-14b	Dj-25	
N°	c2–63	c1–37	2	10	c3–10	c3–73	c4–13	c1–76	c4–34	4	24	
SiO2	35.18	34.7	34.45	45.3	45.62	44.76	45.31	46.9	46.13	46.27	45.04	
TiO2	2.78	2.61	1.47	0.47	0.48	0.29	0.2	0.17	0.13	0.35	0.29	
Al2O3	17.26	16.55	16.12	27.04	28.31	30.42	31.08	32.7	32.34	28.1	30.83	
FeO	23.67	25.47	29.62	7.22	5.92	5.04	5.13	3.34	2.34	4.7	5.56	
MnO	0.38	0.62	0.81	0.45	0.35	0.26	0.29			0.27	0.2	
MgO	6.68	6.42	3.79	2.61	2.17	1.05	0.99	1.3	1.4	2.21	0.79	
CaO	0.1	0			0	0.19	0	0.03				
Na2O	0.18	0.13	0.34	0.35								
K2O	8.81	8.81	9.08	10.41	0.19	0.53	0.3	0.31	0.45	0.34	0.33	
Li2O*	0.51	0.37	0.30	0.63	2.34	1.64	1.68	1.43	1.60	1.81	1.92	
P2O5												
F	0.48	0.97	1.53	1.43	1.05	0.62	0.65	0.47	0.59	0.73	0.8	
Cl	0.08	0.13	0.14			0.05		0.03	0.04	0.04		
"H2O"	3.73	3.54	3.28	3.87	4.01	4.09	4.14	4.28	4.20	4.072	4.075	
"Total"	99.63	99.91	100.29	99.18	100.75	99.44	100.35	99.21	99.69	99.16	99.64	
Structural formula on a (O, OH)12 basis												
Si	2.67	2.60	2.50	2.96	3.03	3.06	3.01	3.12	3.09	3.14	3.03	
Al4	1.33	1.39	1.42	1.04	0.97	0.94	0.94	0.88	0.91	0.86	0.97	
Ti	0.16	0.15	0.08	0.02	0.02	0.01	0.01	0.01	0.01	0.02	0.01	
Al6	0.21	0.07	0	1.05	1.25	1.51	1.53	1.68	1.64	1.39	1.48	
Fe	1.50	1.60	1.85	0.39	0.33	0.29	0.29	0.19	0.13	0.27	0.31	
Mn	0.02	0.04	0.05	0.02	0.02	0.02	0.017	0	0	0.02	0.0	
Mg	0.75	0.72	0.42	0.25	0.22	0.11	0.10	0.13	0.14	0.22	0.08	
Ca	0.00	0	0	0	0	0.01	0	0.00	0	0	0	
Na	0.03	0.02	0.05	0	0	0	0	0	0	0	0	
K	0.85	0.84	0.87	0.03	0.02	0.05	0.03	0.03	0.04	0.03	0.03	
Li*	0.16	0.11	0.09	0.80	0.62	0.45	0.46	0.38	0.43	0.49	0.52	
P	0	0	0	0	0	0	0	0	0	0	0	
F	0.12	0.23	0.36	0.30	0.22	0.14	0.14	0.10	0.13	0.16	0.17	
Fe#	0.665	0.690	0.814	0.608	0.605	0.729	0.744	0.590	0.484	0.544	0.798	

A1), and structural formulas were calculated on a 12 (O, OH) basis. They are typical trioctahedral micas, with a low Al^{VI} component, i.e., with a dominantly annite/phlogopite component. The rather constant Fe/Fe + Mg (Fe#) ratio being in average of 0.68 (Fig. 7), this component is Mg-annite. The ratio is however lower (0.54) for the MME from the biotite granite. When plotting the analyses in the Alt-Si-R^{2+} (*apfu*) triangular diagram of Monier and Robert (1986a) (Fig. 8a), the trioctahedral micas appear to be in fact lithian annite ("protolithionite"), in accordance with their F content (0.48 to 1.85 wt% F). Biotite relicts in the muscovite granite are however closer to the annite pole. Tischendorf et al. (1999) proposed several empirical formulas for estimating the Li_2O content in trioctahedral micas. We here use the Si (apfu)-based estimate, experience having shown that this estimate is the better. Results are presented in Table 1 and Appendix A1, and when plotted in the Li-Alt-R^{2+} triangular diagram of Monier and Robert (1986b) (Fig. 9a), it is seen that they are consistent with that was expected from Fig. 8a.

Dioctahedral micas (Fe-Li muscovite)

White micas from all the granite types were analyzed by EPMA (representative analyses in Table 1 and full data in Appendix A1), and structural formulas were calculated on a 12 (O, OH) basis. The Fe# is quite variable, with an overall average of 0.68. A clear distinction may however be made between the two generations of white micas in muscovite granite, with muscovite 1 (large euhedral flakes) being more magnesian than muscovite 2 (patches in the large flakes, and anhedral white micas in the feldspath macrocrysts and the matrix) (Fig. 7). White micas in the garnet granite and the aplite display compositions typical for muscovite 1, whereas micas from the greisens are in the range of the more iron-rich

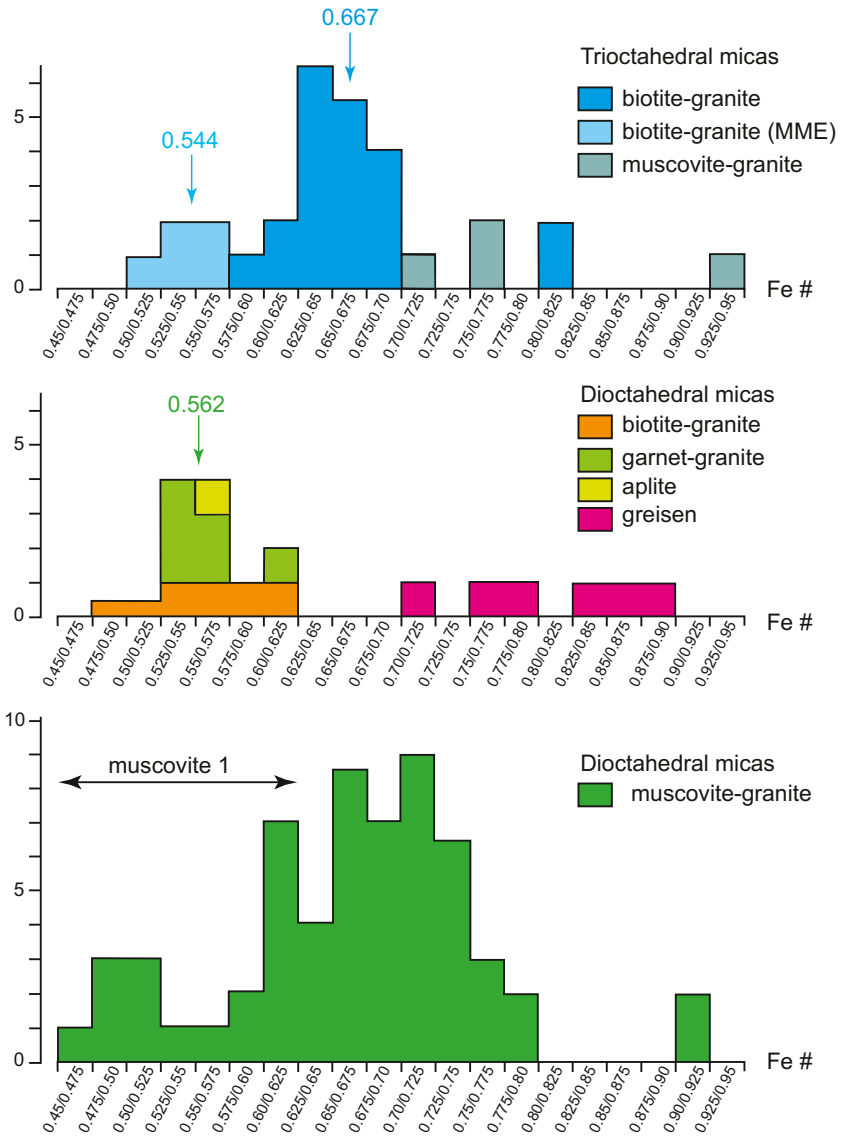

Fig. 7 Histograms of the Fe# (Fe/Fe + Mg) ratio in the micas from the different Djilouet granite facies

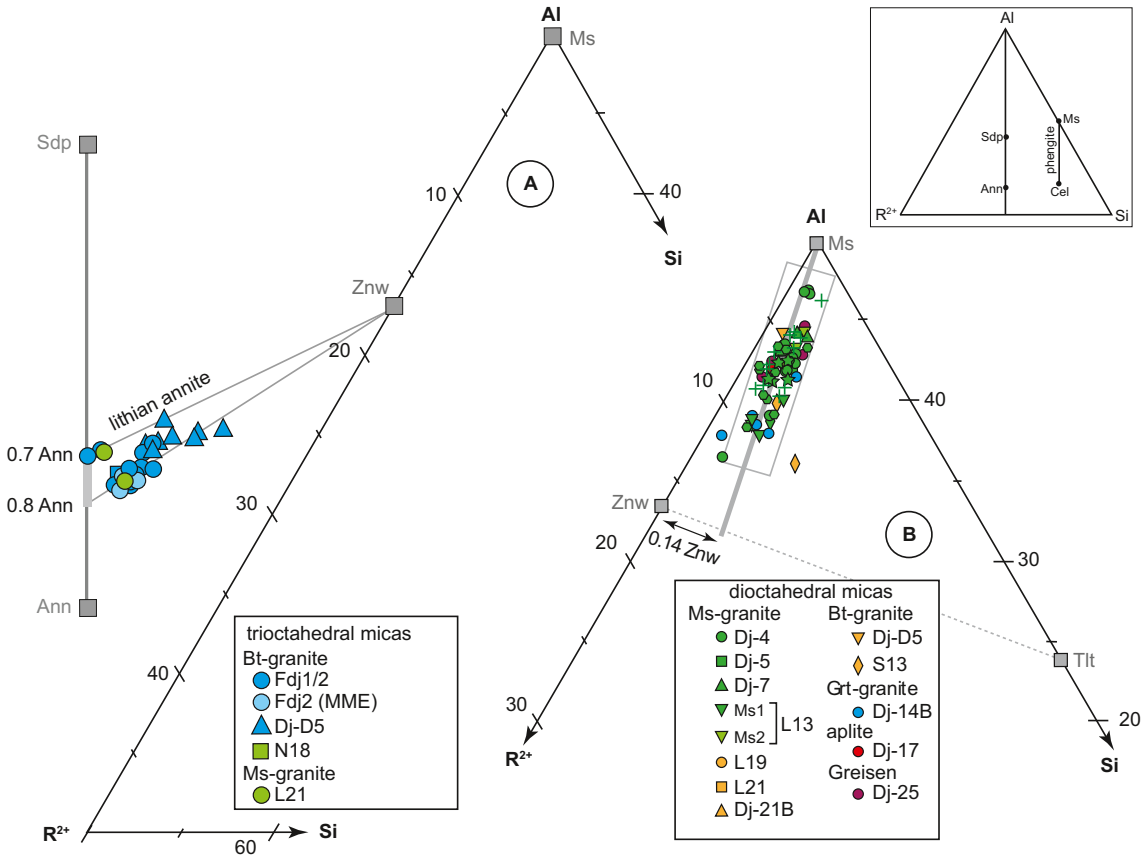

Fig. 8 Projection of the Djilouet micas in the triangular Al-Si-R^{2+} diagram of Monier and Robert (1986a). Insert: the reference triangle. **a** Trioctahedral micas, showing a departure from the annite-siderophylite joint. **b** Dioctahedral micas, showing a departure from the phengite trend

micas from the muscovite 2 generation in muscovite granite. When plotted in the Alt-Si-R^{2+} (*apfu*) triangular diagram of Monier and Robert (1986a), the white micas appear to significantly depart from pure muscovite, forming a trend toward a zinnwaldite-rich intermediate composition between zinnwaldite and trilithionite (Fig. 8b), and may therefore be classified as Fe-Li muscovite. There seems to be a real difference between early and late muscovite (greisen muscovite, secondary muscovite from muscovite granite), the latter being less lithian than the former. The white micas consistently contain F (up to 0.30 wt% F) allowing their Li_20 content to be estimated according to the empirical formula of Tischendorf et al. (1999). The results are presented in Table 1 and Appendix A1. From the data in Fig. 8b, the Djilouet muscovite trend may be predicted in the Li-Alt-R^{2+} triangular diagram of Monier and Robert (1986b), but, as seen in Fig. 9b, the Li content of Djilouet muscovite is clearly underestimated by the Tischendorf et al. (1999) formula, the obtained muscovite trend strongly departing from the expected one, and, what is worse, entering the (forbidden) two-mica field in the diagram (trend 1 in Fig. 9b). This difficulty may be overcome by modifying Tischendorf et al.'s (1999) trial and error empirical formula, in order to make the Li_2O estimates compatible with the expected trend. The results are presented in Table 1 and Appendix A1, and when plotted in Fig. 9b (trend 2), it is seen that they are better consistent with that was expected from Fig. 8a.

Phosphates

Xenotime Xenotime in both muscovite- and garnet-bearing granites are Y-rich varieties, with Y varying between 25.38 and 33.34 wt% and ∑HREE between 3.72 and 16.54 wt%. The analyses may display significant contents in silicium (up to 2.77 wt% Si) and fluorine (up to 2.85 wt% F), inversely correlated to the HREE contents (Table 2). This is due to the vector exchange $P_{-1}O_{-1}Si_{+1}F_{+1}$ allowing the entrance of F into the PO_4 tetrahedra (Bastos Neto et al. 2012). According to Talla et al. (2011) and Abe et al. (2016), OH defects, controlled by Y vacancies, may be present in the xenotime structure, allowing however no more than a few 100 ppm water in the composition, excepted in metamict varieties, in which water content may reach the % level (Talla et al. 2011). This is not however sufficient to explain the low ∑ in the analyses. Yet, when calculated on a (O + F) = 4 basis, the analyses yield rather satisfying structural formulas (Table 2), and a plot of

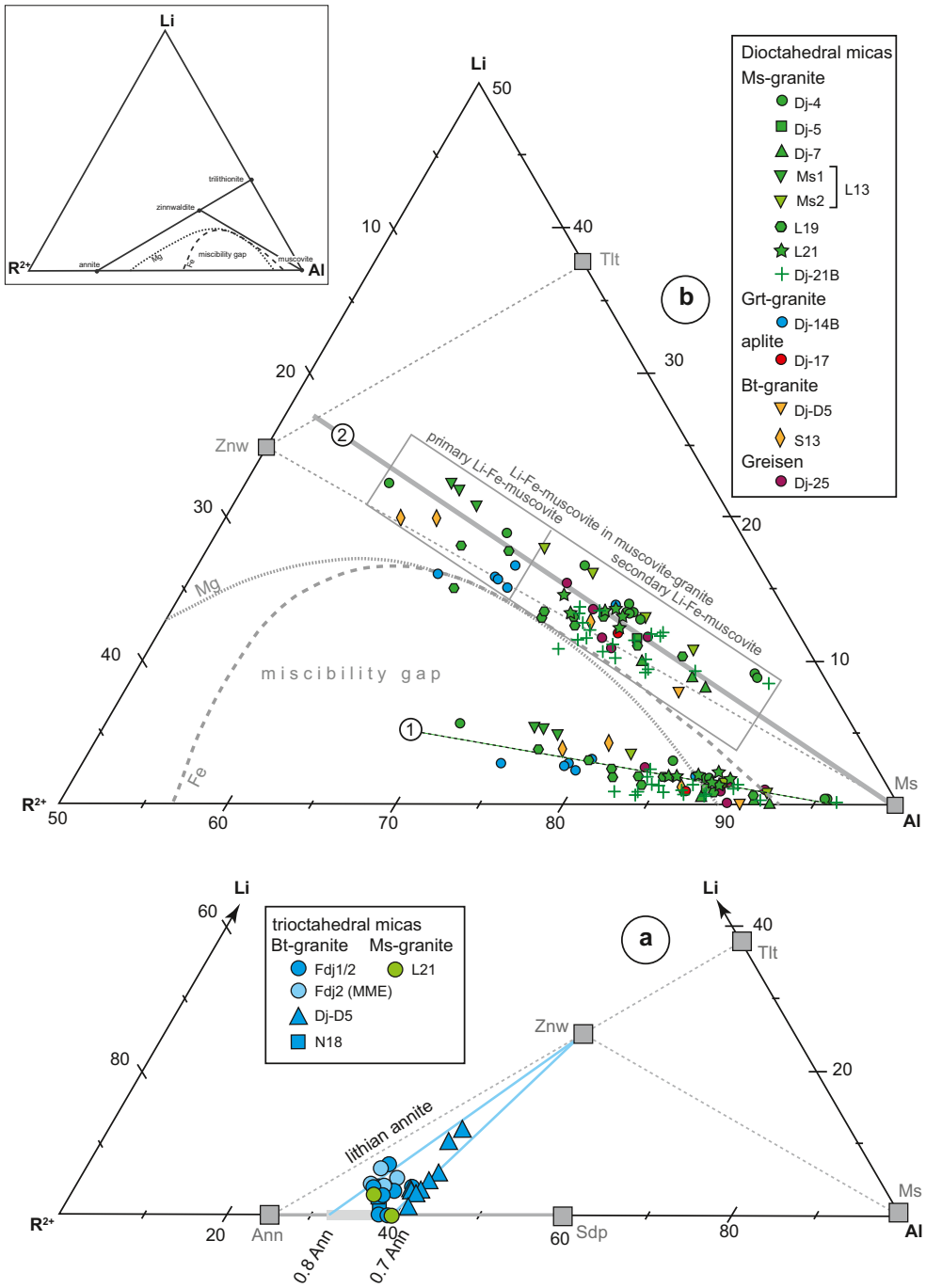

Fig. 9 Projection of the Djilouet micas in the triangular Li-Al-R^{2+} diagram of Monier and Robert (1986a), where the Li content was estimated. Insert: the reference triangle. **a** Trioctahedral micas with Li estimated from the SiO_2 content by the equation $Li_2O^* = (0.287xSiO_2)-9.552$ (Tischendorf et al. 1999); the obtained trend is consistent with Fig. 8b. **b** Dioctahedral micas; (1) the trend obtained with Li estimated from the F content by the equation $Li_2O^* = 0.395xF^{1.326}$ (Tischendorf et al. 1999); this trend is not consistent with Fig. 8b; (2) the trend obtained with a trial and error estimate of the Li content, according to the equation: $Li_2O^* = 0.95 + 1.3F^{1.326}$; this time, the trend is consistent with Fig. 8b

HREE *apfu* or Si *apfu* vs F *apfu* (not shown) yields the expected correlations. It appears that the F-rich Y variety corresponds to the xenotime 2 generation in the muscovite- and garnet-bearing granites.

In the muscovite granite are equally found minerals representative of the xenotime-uranothorite solid solution (Mesbah et al. 2016). All the intermediaries exit between a Th-rich xenotime, with formula $(Ca_{0.02}Th_{0.26})$ $(Y_{0.46}Dy_{0.04})$ $(Si_{0.42}P_{0.58})$ (O3.8 F0.2), and a Y-rich uranothorite with formula $(Ca_{0.01}Th_{0.53}U_{0.48})$ $(Y_{0.08})$ $(Si_{0.89}P_{0.11})$ O_4.

Monazite As seen in Table 2, when calculated on a (P + Si = 1) basis, all the Djilouet monazites are Ce-monazites, with a rather constant Ce/∑REE ratio comprised between 0.41 and 0.62, without significant differences between the granite facies. The monazites mainly differ by their thorium contents, which increase from the muscovite granite, where monazite contains nearly no thorium, to the biotite granite, with an average 6.45 wt% ThO_2 in the monazite, and the garnet-bearing granites, in which the average content in monazite is 16.13% ThO_2. By contrast, the absence of any uranium

Table 2 Representative analyses of the accessory minerals from the Djilouet granites (SEM-EDS analyses)

	Ilmenite	Rutile				"Pyrochlore"					Xenotime	
	Bt-granite	Ms-granite		Bt-granite			Grnt-granite		Ms-granite		Ms-granite	
		Rutile 1		Rutile 2							Xnt1	Xnt2
Sample	Fdj-2	Dj-4	Dj-19	Dj-13		Dj-14b	Dj-14b	Dj-15	Dj-19		Dj-19	Dj-19
N°	spC-1	sp1	sp2	spB-1		spB-1	spC-1	spA-1	sp19-A		spA-2	spA-4
TiO2	50.86	97.05	94.48	84.5	SiO2	3.25	2.77	0.35	3.51	SiO2	0	3.67
CaO	0	0	0.47	0	Na2O	0	0.99	0	0	P2O5	36.1	31.25
FeO	34.81	0	0.78	1.65	P2O5	3.78	0.59	0	0	CaO	0	0
MnO	10.94	0	0	0	CaO	2.23	2.18	0.8	0.66	Y2O3	36.52	42.34
Nb2O5	0	1.65	1.1	1.73	TiO2	13.3	44.8	41.19	23.44	Gd2O3	4.28	0
Ta2O5	0	0.81	1.29	0	FeO	1.84	2.92	4.86	3.00	Dy2O3	6.48	3.84
WO3	0	0.6	0.86	5.93	Y2O3	13.18	6.24	1.85	14.59	Er2O3	4.04	0
					Ce2O3	2.82		0	0	Yb2O3	4.25	3.92
Σ	96.61				Dy2O3	0	0	0	2.03	ThO2	0	0
					Nb2O5	24.96	16.16	15.34	15.74	UO2	0	0
cation b	**2**	3	**3**	**3**	Ta2O5	0		2.09	4.85	F	0	0.94
					WO3	2.51	3.29	3.33	7.92			
Ca	0	O	0.03	0	ThO2	3.36	1.76	0	0	Σ	91.67	85.96
Fe	0.76	O	0.03	0.06	UO2	0.93	4.89	1.33	2.05			
Mn	0.24	O		0						basis (O.F)4)		
Nb	0	0.03	0.02	0.03	Σ	72.16	86.59	87.32	76.25			
Ta	0	0.01	0.01	0						Ca	0	0
W	0	0.01	0.01	0.07	basis:2 cations in site B					Th	0	0
Ti	0.99	2.96	2.91	2.68	site A					U	0	0
0	3.01	5.96	5.99	5.95	Na	0	0.09	0	0	Y	0.68	0.79
					Ca	0.17	0.1	0.03	0.14	Dy	0.07	0.04
					Fe	0.11	0.09	0.1	0.16	Gd	0	0
					Y	0.5	0.15	0.03	0.49	Er	0.04	0
					Ce	0.07	0	0	0	Yb	0.05	0.04
					Th	0.05	0.02	0	0	Si	0	0.13
					U	0.01	0.02	0.01	0.03	P	1.07	0.93
					ΣA	0.93	0.47	0.17	0.82	O	4,00	3.9
					site B					F	0	0.1
					P	0.23	0.02	0	0			
					Si	0.2	0.11	0.01	0.22			
					Ti	0.72	1.5	1.68	1.12			
					Nb	0.81	0.33	0.26	0.45			
					Ta	0	0	0.02	0.08			
					W	0.05	0.04	0.03	0.13			
					site X/Y							
					O	5.9	4.76	4.34	5.57			

	Grnt-granite		"Urano-thorite" Ms-granite			Monazite Bt-granite		Ms-granite Grnt-granite				S-Monazite Ms-granite		"Chernovite" Grn-granite
	Xnt1	Xnt2												
Sample	Dj-14b	Dj-15	Dj-19	Dj-19		FdJ-2	S5-S6	L13	Dj-14b	Dj-14b	L13		Dj-14c
N°	spC-3	spA-1	spA-1	spB-1		spC-2	spA-1	spA-1	spA-1	spB-3	spA-1		spB-1
TiO2	1.32	6.66	10.84	12.27	SiO2	3.1	1.18	0	1.43	0.89	0.65	SiO2	1.43
CaO	35.18	24.77	10.07	1.79	P2O5	27.34	30.15	28.93	21.42	22.25	19.41	P2O5	4.8
FeO	0	1.05	2.56	1.6	SO3	0	0	0	0	0	9.07	CaO	2.95

Table 2 (continued)

MnO	36.92	32.26	12.06	2.08	CaO	0.66	0	0	6.82	4.95	10.03	Y2O3	18.08
Nb2O5	3.21	0	0	0	Y2O3	0	0	0	0	0	0	Ce2O3	4.2
Ta2O5	6.28	4.27	1.65	0	La2O3	13.89	12.19	14.31	2.29	6.26	4.77	Nd2O3	6.1
WO3	3.64	0	0	0	Ce2O3	25.91	26.24	32.49	8.79	21.94	12.62	Sm2O3	3.84
	3.68	0	3.03	0	Pr2O3	0	3.78	3.55	0	2.21	0	Gd2O3	5.49
Σ	0.67	0	26.71	32.07	Nd2O3	7.48	15.98	12.36	4.59	9.42	6.36	Dy2O3	5.46
	0	0	6.04	29.93	Sm2O3	0	3.72	0	0	0	0	As2O3	23.08
cation b	0	3.1	2.07	0	Eu2O3	0	0.17	0	0	0	0	F	1.89
					Dy2O3	0	0	0	1.01	0	0		
Ca	90.94	72.11	78.27	79.74	Gd2O3	0	2.61	0	0	0	0	Σ	77.32
Fe					PbO	0	0	0	0.89	0	2.02		
Mn			basis (Si + P = 1)		ThO2	11.05	4.51	2	28.96	10.27	15.94	basis (AsO4)	
Nb					UO2	0	0	0	0	0	0.91		
Ta	0	0	0.01	0.01								Ca	0.18
W	0	0	0.3	0.53	Σ	89.43	100.52	93.64	76.2	78.46	81.78	Y	0.53
Ti	0	0	0.07	0.48								Ce	0.09
0	0.68	0.65	0.4	0.08	base (P + Si + S) = 1							Nd	0.12
	0.07	0.05	0.03	0								Sm	0.07
	0	0	0.05	0	Ca	0.03	0	0	0.37	0.27	0.45	Gd	0.1
	0.04	0	0	0	Pb	0	0	0	0.01	0	0.02	Dy	0.1
	0.04	0	0	0	Th	0.1	0.04	0.02	0.34	0.12	0.15		
	0.05	0.22	0.58	0.89	La	0.2	0.17	0.22	0.04	0.12	0.01	Si	0.08
	1.04	0.79	0.42	0.11	Ce	0.36	0.36	0.49	0.16	0.41	0.07	P	0.23
	4,00	3.63	3.7	4.4	Pr	0	0.05	0.05	0	0.04	0.19	As	0.78
	0	0.37	0.25	0	Nd	0.1	0.21	0.18	0.08	0.17	0.1	O	3.58
					Sm	0	0.05	0	0	0	0	F	0.33
					Eu	0	0,00	0	0	0	0		
					Dy	0	0	0	0.02	0	0		
					Gd	0	0.03	0	0	0	0		
					Si	0.12	0.04	0	0.07	0.04	0.03		
					P	0.88	0.96	1	0.93	0.96	0.69		
					S	0	0	0	0	0	0.28		
					O	3.65	3.91	3.94	4.01	4.45	3.97		

content is striking. Concomitantly with the elevated thorium contents, the monazite is hydrated, as shown by the low analytical sums in Table 2. Excepted in the garnet-bearing granite, in which it may contain significant calcium contents (up to 6.82 wt% CaO), the Djilouet monazite is Ca-poor.

By contrast, a few monazite crystals that are enriched in S are also Ca-rich. These monazites were found as secondary products in the muscovite granite (see above). Sulfur (and a minor arsenic) enters the monazite structure as clinoanhydrite substitution (Uher et al. 2007), and accordingly the S-rich monazite displays the average structural formula $(Ca_{0.46}Pb_{0.02}Th_{0.17})$ $(La_{0.07}Ce_{0.19}Nd_{0.09})$ $(Si_{0.01}As_{0.01}P_{0.74}S_{0.24})$ $O_{3.96}$.

Nb-Ti-Y-REE-Th oxides: pyrochlore supergroup

The complex Nb-Ti-Si-Y-REE-Ca-Fe-U-Th oxides found in the garnet and muscovite granites display typically low analytical sums (Table 2), meaning that they may be members of the pyrochlore supergroup. Minerals of this supergroup have the structural formula $A_{2-m}B_2X_{6-w}Y_{1-n}$ (Atencio et al. 2010), where A is a [8]-coordinated cation (Na, Ca, Fe, Y, REE, U, Th) or H_2O, B is a [6]-coordinated cation (Ta, Nb, Ti, W, Si, P), X is O (with subordinate OH and F), and Y is OH, F, O, or H_2O. When calculated on the basis of 2 cations in the B site, the complex Djilouet Nb-Ti oxides fit rather well to this structural formula (Table 2). With an m parameter comprised between 0.85 and 1.83, H_2O is likely to be present in the A-site (Atencio et al. 2010). However, owing to the U-Th contents, a significant part of the H_2O responsible for the low analytical sums is likely to be present under an adsorbed form, due to the metamictization (Atencio et al. 2010). In all the analyses, Ti is the dominant cation in site B, and Fe is the dominant cation in site A, thus the Djilouet niobo-titanates may be classified as hydrated ferroan betafite, with additional Ca and U-Th (U/Th close to 1) in site A, and a significant Si content (0.1 to 0.2 *apfu*) in the site B, whereas Ta is only a very minor component.

Geochemistry of the Djilouet suite

Major elements

Bulk rock analyses are presented in Table 3.

All the facies share common characteristics: highly siliceous, with SiO_2 contents between 71.57 (in a biotite granite)

Table 3 Major (wt%) element for the granites from Djilouet cupola

Rocks sample	Coarse biotite granite			Muscovite granite							Garnet-bearing granite			Smoked quartz granite	Aplitic veins		
Sample	FDj1	FDj2	18	4	05	6	7	21	23	FDj3	14	14b	14b2	15	8	17	24
SiO2	71.94	71.57	73.57	73.55	78.1	79.07	76.3	74.86	76.93	72.93	73.86	74.64	77.51	76.12	72.99	74.2	76.21
TiO2	0.25	0.24	0.09	0.09	0	0.05	0.05	0.06	0.06	0.05	0.05	0.05	0	0.05	0	0	0.06
Al2O3	15.11	14.88	12	13.25	12.93	12.38	13.86	14.65	12.93	14.94	14.47	14.19	13.4	13.18	14.81	13.97	13.84
Fe2O3	2.45	2.5	3.16	2.65	0.2	0.2	0.1	1.09	0.54	0.33	1.08	0.91	0.31	2.03	0.35	1.91	1.37
MnO	0.05	0.06		0.01	0.01	0	0	0.06	0	0	0.01	0.02	0.02	0	0	0.02	0
MgO	0.57	0.59	0.21	0.23	0.3	0	0	0.2	0.14	0.26	0.15	0.11	0.03	0.09	0	0	0.16
CaO	1.79	1.47	0.44	0.33	0.35	0.22	0.38	0.62	0.3	0.28	0.36	0.23	0.28	0.24	0.57	0.17	0.37
Na2O	2.42	3.31	1.56	3.46	3.44	2.49	2.77	2.91	2.73	3.42	3.68	4.24	3.86	3.26	5.77	2.83	2.74
K2O	3.92	3.9	5.48	4.97	5.33	4.36	4.19	4.66	4.4	6.52	5.18	5.1	5.12	4.75	3.7	4.23	5.14
P2O5	0.05	0.09	0	0.06	0	0	0	0	0	0	0.06	5.18	0	0	0.07	0	0
F	0	0	0	0	0.02	0	0	0.39	0	0	0	0	0.06	0	0	0	0
LOI	0.99	0.83	2.1	1.59	0.57	0.86	1.01	1.83	1.91	0.5	1.09	0.56	0.47	1.57	0.73	0.33	0.64
Total	99.54	99.44	98.61	100.19	101.25	99.63	98.66	101.33	99.94	99.23	99.99	105.23	101.06	101.29	98.99	97.66	100.53
O_F	0	0	0	0	0.01	0	0	0.16	0	0	0	0	0.03	0	0	0	0
CTotal	99.54	99.44	98.61	100.19	101.24	99.63	98.66	101.17	99.94	99.23	99.99	105.23	101.03	101.29	98.99	97.66	100.53
ACNK	1.32	1.21	1.29	1.14	1.07	1.34	1.42	1.34	1.32	1.13	1.17	1.1	1.08	1.2	1.02	1.46	1.29
ANK	1.84	1.54	1.41	1.20	1.13	1.4	1.52	1.49	1.4	1.18	1.24	1.14	1.13	1.25	1.1	1.51	1.37
A	71.23	49.85	53	30.98	16.99	62.08	79.97	72.41	61.42	34.29	42.27	25.04	19.61	43.92	5.44	86.84	60.73
B	47.95	48.95	45.92	40.03	9.94	3.13	1.88	19.36	10.98	11.21	17.88	14.76	4.62	28.28	4.38	23.92	21.88
Q*3	51.8	42.6	53.2	38.3	37.6	57.9	57.9	51.2	54.3	32.6	38.4	32.9	36.1	45	23.5	57.6	49.6
B*3	−7	−2.5	−3.8	−0.1	−1.8	−12	−15.9	−11.5	−10.7	−5.1	−5.7	−2.8	−3.1	−4.4	−0.4	−14	−8.7
F*3	55.2	59.9	50.5	61.8	64.2	54.1	58	60.3	56.4	72.5	67.3	69.9	67	59.4	76.9	56.4	59.2

The bulk rock analyses were performed at the ORGM-Laboratory (Boumerdes, Algeria). Only three samples (05, 21, 14b2) could be completely analyzed (major and trace elements) at the SARM l-Laboratory at the CRPG-Nancy

and 79.07 (in a muscovite granite); highly potassic with K_2O/Na_2O ratios between 1.20 (in a muscovite granite) and 3.51 (in a biotite granite) and averaging 1.64 (to the exception of a low ratio in one aplite); poor in calcium, the CaO content being consistently ≤ 0.6 wt%, to the exception of two biotite granites, with 1.47 and 1.79 wt% CaO, respectively; low in mafic components, with $Fe_2O_3 + MgO + TiO_2$ comprised between 0.15 (in a muscovite granite) and 3.46 (in a biotite granite), i.e., they are all leucogranites; low in magnesium with the M index of Hughes and Hussey (1976) (M = 100 Mg/Mg + ∑Fe) comprised between 0 and 75, but being in most cases lower than 35; and very low in phosphorus, with P_2O_5 being consistently below the detection level (*bdl*), and never exceeding 0.1 wt%.

The Djilouet granites mainly differ by their relative aluminum contents, with A/CNK comprised between 1.08 and 1.46 and A/NK between 1.1 and 1.84, i.e., from compositions close to the metaluminous/peralkaline/peraluminous triple point to mild peraluminous compositions, in the A/NK vs A/CNK diagram (Fig. 10). This is however, in part due to the effects of alteration, the development of muscovite at the expense of other biotite or feldspars having for effect to increase in strong proportion the relative aluminum content of this altered rocks. This is well seen on the diagrams in Fig. 11 (AB diagram of Debon and LeFort 1988, and $Q^*_3B^*_3F^*_3$ diagram of De La Roche et al. 1980), which are particularly well fitted to untangle the effects of alteration and of primary magmatic evolutions. When the effects of alteration are taken into consideration, it is seen in Fig. 11 that the Djilouet suite roughly defines an evolution trend, between the peraluminous and more mafic biotite granites and the aplites, with the muscovite- and garnet-bearing granites in an intermediate position.

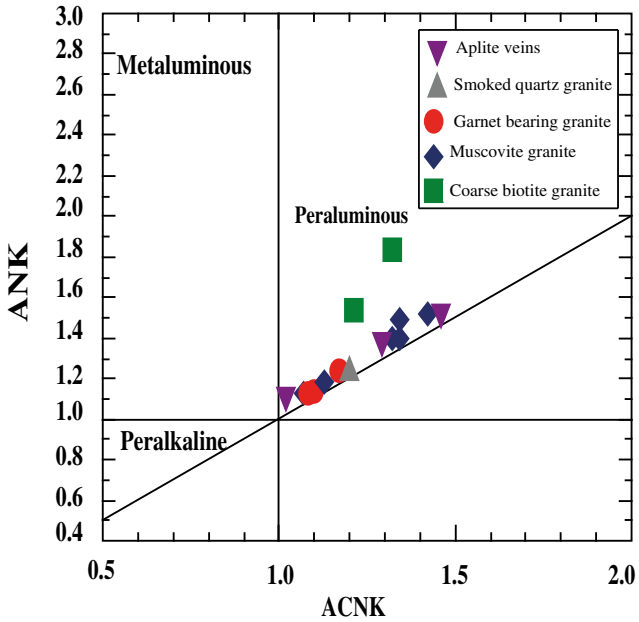

Fig. 10 Projection of the different facies of the Djilouet suite in the A/NK vs A/CNK diagram (Maniar and Piccoli 1989)

Trace elements

Trace elements and the REE could only be analyzed in three samples, two from the muscovite granite and one from the garnet-bearing granite. The data are given in Tables 4 and 5. Despite this limited data base, the obtained information allows interesting observations.

Trace elements

As shown in Fig. 12, the muscovite- and garnet-bearing granites of the Djilouet suite display rather similar trace element patterns. In accordance with their evolved major element compositions, they are depleted in Ba and Sr and enriched in Rb. This is classically interpreted as the result of strong fractionation (El-Bouseily and El-Sokkary 1975). However, the relatively low K/Rb ratios (127 to 162) may be indicative of secondary (subsolidus) remobilization with Rb input (Irber 1999), thus complicating the interpretation of the Rb content. In this connection, it is observed that Cs concentration does not systematically follow the Rb behavior (Fig. 12). For a series of elements, the Djilouet muscovite- and garnet-bearing granites are in the range of the peraluminous low phosphorus rare metal granites (PLP-RMG) as defined by Linnen and Cuney (2005). Such are Zr, Hf, Y, Th, and U. In particular, the Hf/Zr and Th/U Djilouet ratios (0.06 to 0.1 and 1.8 to 2.9, respectively) are in the half lower part of the corresponding PLP-RMG ranges. By contrast, they are enriched in both Th and U relatively to the central Hoggar Taourirt granites (Azzouni-Sekkal 1995). It is therefore surprising to observe that niobium and tantalum are not highly concentrated in the Djilouet granites, with Ta + Nb comprised between 10.4 and 17.1, far lower than in PLP-RMG (40 to 160 ppm: Linnen and Cuney 2005). What is more, the Ta/Nb ratio, comprised between 0.17 and 0.34, is exceptionally low. When the other rare metals are considered, it is found that their behavior is contrasted. Tungsten, moderately concentrated in the muscovite granites (7–17 ppm W), is rather high in the garnet-bearing granite (55 ppm W). Lithium and tin, on the other hand, display the same behavior, being poorly concentrated (Li: 7–13 ppm, Sn 7–8 ppm), excepted in one of the two muscovite granite (samples 21), which is particularized by strong enrichment, not only in Li (110 ppm) and Sn (160 ppm) but also in As, Pb, and Bi (Fig. 12). It is also the one in which Rb and Cs are the most concentrated (Fig. 12). Significant subsolidus reworking may thus be suspected in this sample, and the conclusion will remain that the evolved granites of the Djilouet suite are poorly enriched in rare metals. This is the most surprising in view of the accessory mineral assemblages in which Nb, Ta, or W is present.

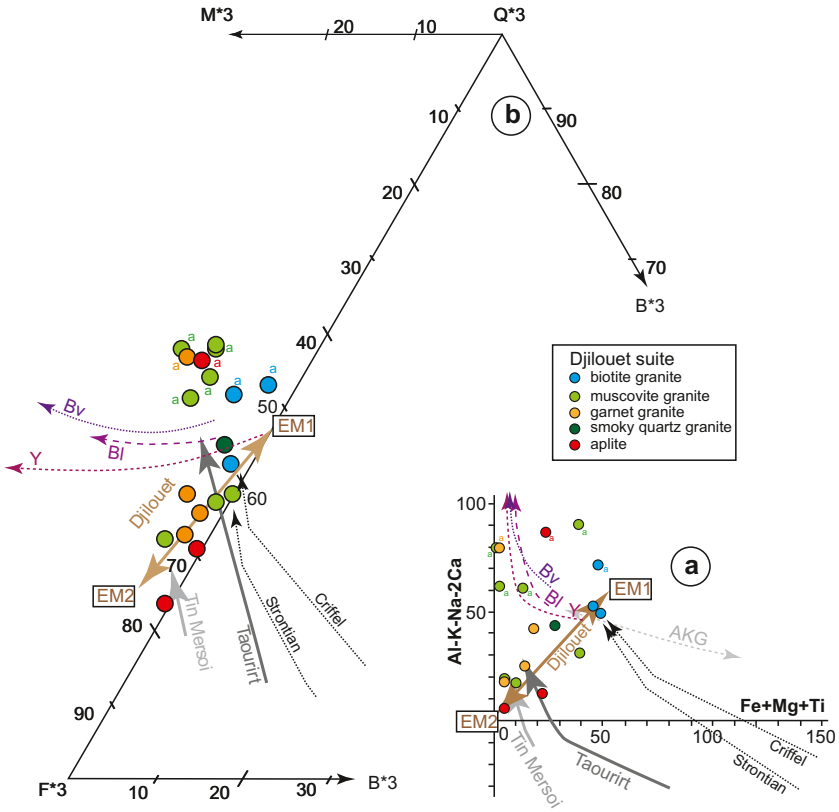

Fig. 11 The Djilouet suite in **A**, the AB diagram (Debon and LeFort 1988), and B, the $Q^*_3B^*_3F^*_3$ diagram of De La Roche et al. (1980). **a** Altered facies are drawn for comparison the evolution trends of (i) A-type granite suites in the Hoggar (Taourirt and Tin Mersoi suites) and (ii) rare metal granite suites from the French Massif Central (Bl Blond suite; Bv Beauvoir suite) and the SE China (Y Yichun suite). EM1, EM2: hypothetical granite end-members (see text for explanation). AKG (for Alumino-Potassic Guéret type) trend: possible mixing trend between the EM1 and a mafic melt typified by the MME enclaves in the biotite granite (see text for explanation). Data for the reference trends: Azzouni-Sekkal et al. (2003), Fowlers et al. (2008), Lin et al. (1995), Raimbault et al. (1995), Soufi (1988)

Rare-earth elements

In the Djilouet muscovite- and garnet-bearing granites, the total REE content is in the 57 to 84 ppm range, i.e., in the lower range of PLP-RMG (11–240 ppm: Linnen and Cuney 2005), lower than in most Taourirt granites in central Hoggar (84–415 ppm: Azzouni-Sekkal and Boissonnas 1993; Azzouni-Sekkal 1995). The REE patterns are very similar for the three granites, being typically wing-shaped ($La_N/Yb_N \approx 1.36–2.93$), with a strong negative Eu anomaly ($Eu_N/Eu_N^* \approx 0.06–0.13$) (Fig. 13a). They may be compared with those of some Taourirt granites, such as the Teg Orak alaskites or the evolved facies of the Isseddienne massif (Azzouni-Sekkal 1995). The patterns display a small tetrad effect, most noticeable in the third tetrad, although the statistical test (Ti indexes of Monecke et al. 2002) is not decisive (Fig. 13a). This effect is consistent with the non-CHARAC behavior (Bau 1996) of the evolved Djilouet granites (Fig. 13a).

Sn-W mineralization

The Djilouet Sn-W mineralization consists in two systems of veins: large quartz veins with wolframite are associated with sets of subparallel quartz veinlets or stockworks with cassiterite (Fig. 14a). All quartz veins and veinlets exhibit symmetric greisenized walls, extending on a few cm (from 1 to 10 cm). Based on a sampling realized by SONAREM work teams in 1986, it was possible to draw a map of iso-contents in tin and tungsten (Fig. 15). As clearly seen, there is a disjunction between tin and tungsten distributions, with tungsten occupying the north-west and tin the south-east of the Djilouet massif. The large greisen strips are otherwise concentrated in south-east part of the massif (compare with Fig. 3). The overlapping between the two systems seems very limited.

Quartz-wolframite veins

The veins strike NE-SW (N10°-40°E) and are subvertical (70° to 85°E). They may reach 700 m in length with a thickness comprised between 10 and 50 cm. Wolframite is the only mineral with the quartz. It forms large (up to 5 cm) euhedral crystals mostly growing orthogonally from the vein border and locally overprinted by quartz testifying for a crack-seal phenomenon at the mineralization time.

Quartz-cassiterite veinlets and stockworks

The system mainly consists in thin subparallel veinlets (1–8 cm) striking NE-SW, locally complicated its suborthogonal veinlets forming stockwork. Cassiterite is euhedral, with a dipyramid habit, and may reach 1 to 2.5 cm. It grows from

Table. 4 Trace element (ppm) compositions of the muscovite granite and garnet granite from the Djilouet suite

Rocks sample	Muscovite granite		Garnet-bearing granite
Sample	05	21	14b2
Ba	45.3	157.5	84.49
Rb	260.2	482.4	265.9
Sr	24.13	46.5	36.02
Y	43.05	34.56	39.34
Zr	29.24	54.84	46.26
Nb	7.77	12.99	9.69
Ta	2.62	4.1	1.69
Th	10.73	15.25	18.89
Ga	20.64	28.6	21.46
Zn	20.48	59.8	11.16
Cu	35.75	25.76	7.55
Hf	2.88	3.29	3.25
Sc	2.97	6.67	4.61
Li	7	109	12.9
Be	3.15	4.45	2.94
U	5.91	5.46	6.45
W	6.66	16.62	54.97
Sn	6.04	161.1	8.43
Cr	74.1	68.34	115.5
Co	0.41	1.17	0.41
Cs	4.85	31.61	6.69
Mo	2.22	2.5	3.47
Ni	0	0	0
Pb	46.28	111.83	39.78
V	3.51	5.73	3.71
As	24.16	120.2	24.64
Bi	0.32	3.49	0.26
Cd	0	0	0
Ge	2.36	3.44	2.23
In	0	0.09	0

Table 5 Rare-earth element compositions (ppm) of the muscovite granite and garnet granite from the Djilouet suite

Rocks sample	Muscovite granite		Garnet-bearing granite
Sample	05	21	14b2
La	7,42	14,64	12,1
Ce	14,14	22,25	27,83
Pr	1,78	2,91	3,61
Nd	7,04	10,87	13,62
Sm	3,5	3,61	4,41
Eu	0,09	0,16	0,1
Gd	5,07	4,04	4,55
Tb	1,1	0,8	0,94
Dy	7,43	5,45	6,78
Ho	1,45	1,16	1,47
Er	3,72	3,14	3,98
Tm	0,57	0,5	0,61
Yb	3,78	3,47	4,26
Lu	0,52	0,51	0,62
Somme	57,61	73,51	84,88
Eu/Eu*	0.06	0.13	0.07
La_N/Yb_N	1.36	2.93	1.97
La_N/Sm_N	1.33	2.55	1.72
Gd_N/Yb_N	1.11	0.96	0.88
Ce/Ce*	0.94	1.07	0.81
Pr/Pr*	1.01	1.12	0.99
TE_1	0.97	1.10	0.90

$Eu/Eu^* = Eu_N / (Sm_N \times Gd_N)^{1/2}$. $Ce/Ce^* = Ce_N / (La_N^{2/3} \times Nd_N^{1/3})$. $Pr/Pr^* = Pr_N / (La_N^{1/3} \times Nd_N^{2/3})$. Degree of the tetrad effect: $TE1 = (Ce/Ce^* \times Pr/Pr^*)^{1/2}$ (Irber 1999)

the vein boundary. Although it is optically zoned, it is homogeneous and devoid of minor elements when analyzed by SEM-EDS. It may contain small euhedral albite laths (Fig. 14. f). Wolframite is only on minor amount in the quartz veinlets.

The wolframite composition was determined by the curve proposed by Sasaki (1959). It illustrates the relationship between Δ ($d_{011} - d_{110}$) and composition in mol.% $MnWO_4$ (Soéda et al. 1979). The Djilouet wolframite is of ferberite composition (curve not shown). Nevertheless, the obtained H/F [hubnerite ($MnWO_4$)/ferberite ($FeWO_4$) ratio)] varies from 8 to 48%. The highest ratio characterizes the wolframite from stockwork with cassiterite close the garnet granite, whereas the lowest H/F wolframite ratio was obtained from the largest mineralized veins in the central part of the deposit.

Discussion

Timing of magmatic and post-magmatic events in the Djilouet massif

The Djilouet pluton clearly overprinted two NE-SW trending ductile shear zones (Fig. 2). One of these shear zones was injected by syn-cinematic leucogranitic ptygmatitic veinlets (Fig. 3), making it likely coeval with the activity of the Tin Amali Shear Zone (TASZ), which is indeed highly migmatitic (Fezaa et al. 2010). The geometry of the giant Tin Amali dyke swarm (Lamri et al. 2016) strongly suggests that they were emplaced in tension cracks coevally with the activity of the TASZ. The Djilouet pluton, as well as the similar Edjéreou and Edjédjé plutons, would therefore have been emplaced later than 558 ± 5 Ma, the age of the Tin Amali swarm, but evidently before the unconformable emplacement of the Late Cambrian Tassili formation. These three plutons would indeed represent the latest Pan-African granite magmatism in the Djanet terrane and could have been coeval with the Late

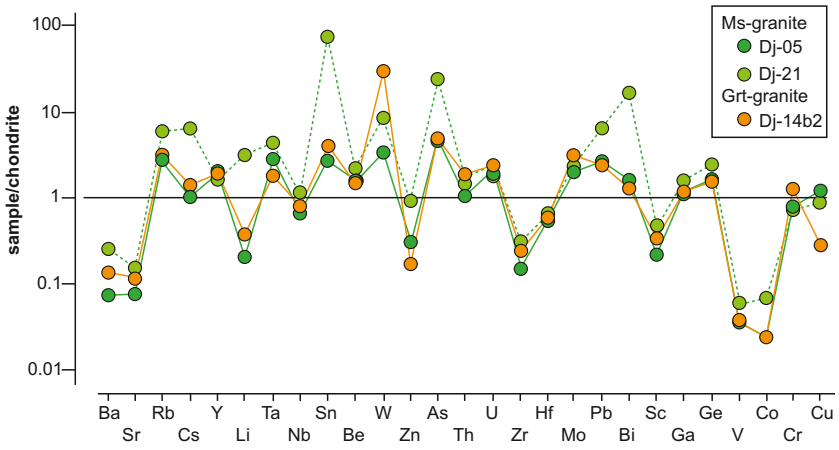

Fig. 12 Spidergram of the trace elements in Djilouet muscovite- and garnet-bearing granites. Normalized to the upper continental crust (normalization data from Rudnick and Gao 2003. excepted Li. from Teng et al. 2004)

Ediacaran Taourirt-RMG event in the central Hoggar (Bechiri-Benmerzoug et al. 2017).

The earliest alteration recorded in the Djilouet pluton was greisenization and the associated muscovitization events, Known to be high temperature processes (≥ 400 °C) (e.g., Cerny et al. 2005), owing to the absence of high temperature events post-dating the Pan-African period in the whole Hoggar, to the exception of a very limited mafic magmatism during the Carboniferous (Bechiri-Benmerzoug et al. 2017). This first alteration episode, and the associated Sn-W mineralization, may have been coeval with the extensive Early Cambrian hydrothermal activity recorded by Rb-Sr and ^{39}Ar-^{40}Ar ages in the granites of the central Hoggar (Bechiri-Benmerzoug et al. 2017). Crystallization of arsenopyrite in some granites may tentatively be related to these episodes.

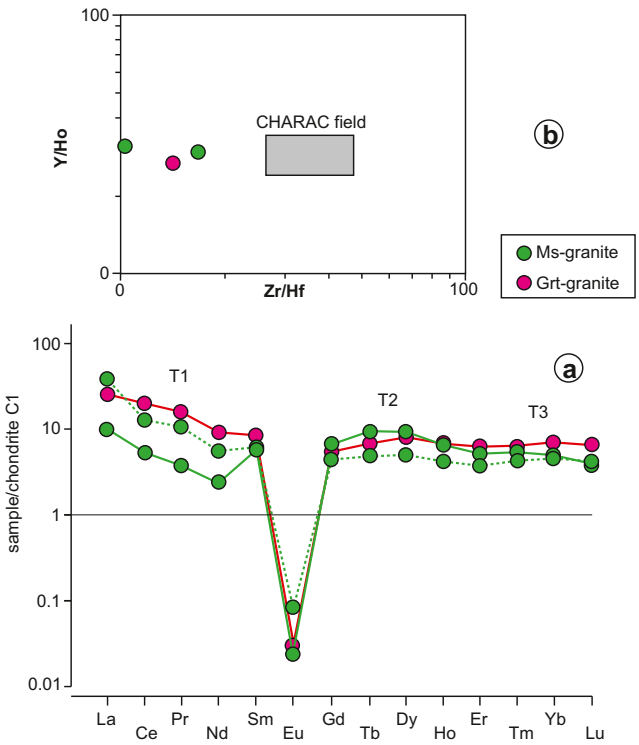

Fig. 13 **a** REE spidergrams for the muscovite- and garnet-bearing granites (normalization to the C1 chondrite of Anders and Grevesse 1989). The patterns display a faint but clear tetrad effect in particular in the third tetrad. **b** Y/Ho vs Zr/Hf diagram (Bau 1996) showing the non-CHARAC behavior of the muscovite- and garnet-bearing granites

At least three later hydrothermal episodes are recorded in the Djilouet pluton, overprinting by BMS sulfides (pyrite, chalcopyrite, Ag-bearing galena) occurred in the granites without apparent associated alteration. This mineralization was not found in the outcropping vein system but was encountered in some drill holes (SONAREM 1986). A low-temperature event, which is attested by the development of kaolinite at the expense of muscovite, was clearly associated with the development of scorodite at the expense of arsenopyrite and an intense remobilization of the REE and actinides (Th. U), with the expression of a series of minerals, including members of the pyrochlore supergroup, S-bearing monazite and arsenates of Y-REE. Development of a Mg-siderite, possibly coeval with fluorite (and the expression of REE fluorides) or formation of an epidote of the allanite group and possibly also with chloritization of the protolithionite, seems to have been the latest hydrothermal event (a faint propylitization), overprinting all the other alteration assemblages. The CO_2 for this late carbonate may have been provided either by the maturation of the Silurian black shales of the Tassili sedimentary pile, or through the Cenozoic mafic volcanism. In the former case, the event would have been related to the Late Cretaceous generalized subsidence of the Hoggar area and passing of the Silurian black shales through the oil and gas windows (e.g., Rougier 2012). In the latter case, it would have coincided with the Djanet volcanism at 8.4–6.8 Ma (Liégeois et al. 2005). The other hydrothermal events post-dating greisenization must therefore have taken place between the Late Paleozoic (since some hydrothermal activity is attested by rejuvenation ages in the Tin Amali dyke swarm: Fezaa et al. 2010) and during either the Mesozoic only (first option) or the Mesozoic and the Cenozoic (second

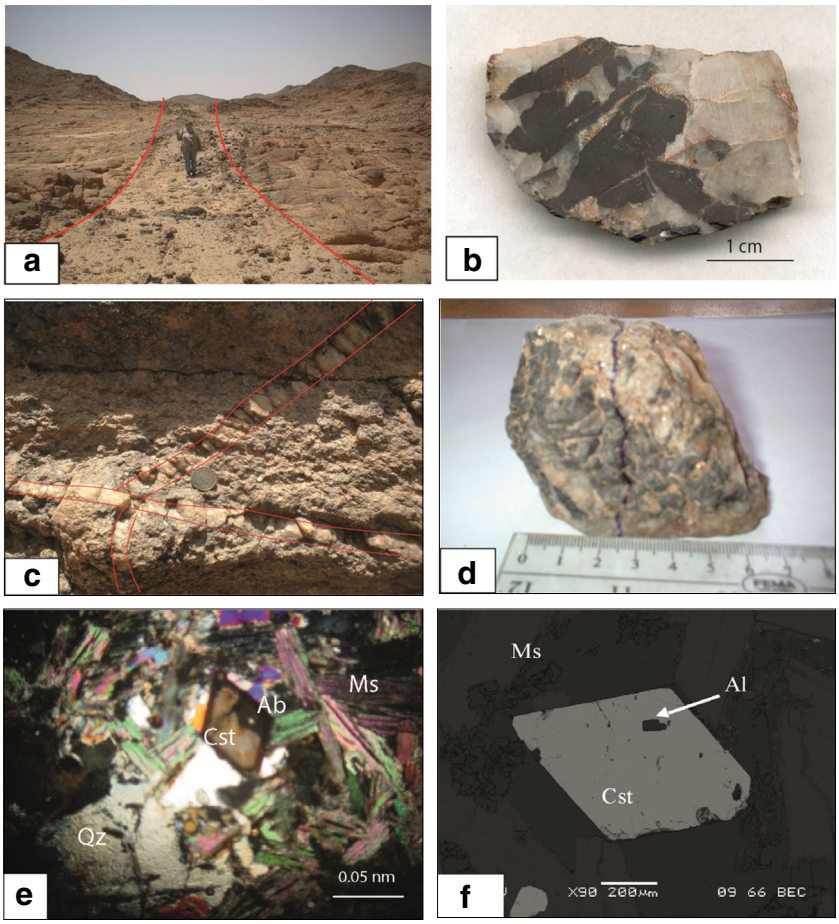

Fig. 14 Aspects of the Sn-W mineralization. (**a**) Panoramic view of W-quartz veins. (**b**) Wolframite in W-quartz veins. (**c**) Cassiterite stockworks mineralized. (**d**) Sn-quartz veins with greisenized wall rocks forming stockworks. (**e**) Bipyramidal cassiterite with albite inclusion observed in LP. (**f**) Bipyramidal cassiterite with albite inclusion observed in SEM

option), although the first option seems more probable, judging from the small global volume of the magmatic products in the Djanet area (6 km^3: Liégeois et al. 2005).

Interpretation of the magmatic trends

The Djilouet trend as the result of a mixing process

At first glance, the "Djilouet trend" observed in Fig. 11 may be interpreted as representative of a typical S-type trend, characterized by the progressive fractionation of ferro-magnesian minerals (mainly the peritectic garnets and/or cordierite issued from the dehydration melting process at the origin of S-type melts), and the presence of garnet-bearing granites in the suite could be taken as further evidence. There are however serious objections to this interpretation. In the first place, it appears (i) that garnet is absent from the less fractionated member of the suite, i.e., the biotite granites, and (ii) that the apparently similarly fractionated muscovite- and garnet-bearing granites mainly differ precisely by the presence of garnet only in the latter. This is difficult to reconcile with the S-type fractionation process. In the second place, the Li enrichment observed in the micas of the suite, and in particular in the primary white micas (Ms 1), is equally difficult to explain by this process. Finally, the contrast between the accessory mineral assemblages of the biotite granite on one hand (ilmenite, apatite, zircon, Th-Ce-monazite) and the muscovite and garnet-bearing granites (Nb-rutile, zircon with Hf-enrichment, Ce-monazite, xenotime, and uranothorite) is particularly difficult to reconcile with the S-type fractionation process.

The only alternative interpretation of the linear Djilouet trend is therefore to consider a mixing process between two distinct end-member granitic melts: EM1 and EM2. As shown in Fig. 11, one of the end-members in this mixing process (EM1) would be close to the less evolved biotite granites, and the other (EM2) could be represented by the aplites, whereas the muscovite- and garnet-bearing granites would result from a mixing dominated by the latter. Some observations at the mineralogical scale may come in support of this interpretation. For example, in the biotite granite, the apparently abrupt transition from an oligoclase core to an albite rim in the plagioclase macrocrysts, or the Th- and Y-rich

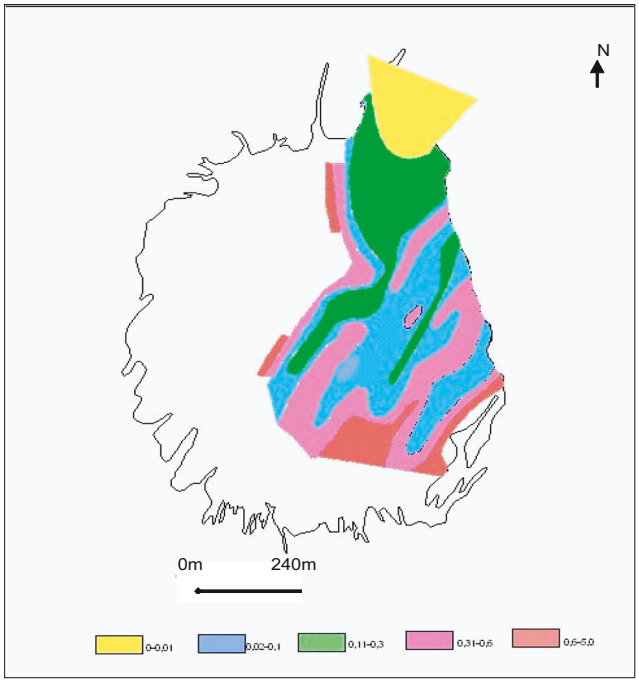

Fig. 15 Map of the Sn/WO_3 ratio distribution in the Djilouet massif. Redrawn from Oulebsir and Kesraoui (2006) and Oulebsir (2009) (based on a SONAREM report for 1986)

assemblages rimming early monazite, may well record interaction of EM1 with some increments of EM2. In the same way, ilmenite inclusions in rutile or apatite from muscovite granite may be seen as remnants of the EM1 component and the xenotime rims corroding zircon-monazite assemblages in both muscovite- and garnet-bearing granite as recording interaction of the EM2 melt with EM1-related xenocrysts.

On the other hand, the apparent depletion in rare metals which has been observed in both the muscovite- and the garnet-bearing granite, when compared with their possible analogues (PLP-RMG. Taourirt granites), could be readily interpreted as the results of a dilution in a less fractionated EM1 end-member.

Nature of the end-members

By comparison with the reference trends in Fig. 11, the EM2 end-member may be representative of highly fractionated melts of the Taourirt family and, in particular, of the Tin Mersoi type. The latter is, in central Hoggar, representative of Taourirt melts with affinity to peralkaline suites (Azzouni-Sekkal 1995. Azzouni-Sekkal et al. 2003). Such an interpretation is consistent with the wing-shaped REE pattern of the muscovite- and garnet-bearing granites and with the high Th/U ratios in these granites. It is also consistent with the high Nb/Ta ratio and the presence of early Nb-rutile in the assemblages of these granites. It however does not explain the differences in the mineralogical cortege between these two granite type, with garnet and abundant xenotime in the garnet-bearing granite. It would seem that the EM1 would itself record several sources, including dehydration melting of a biotite, leading to the production of a peritectic garnet.

At first hand, by comparison with the central Hoggar, where mixing between evolved A-type Taourirt and true RMG has been documented (Marignac et al. 2016), the EM1 end-member could tentatively be compared with the less evolved terms of peraluminous intermediate-phosphorus rare metal granites (PIP-RMG), as defined by Linnen and Cuney (2005) and as exemplified by the Yichun trend in Fig. 11. However, this seems to be contradicted by the very low P contents in the biotite granites, up to 0.09 wt% P_2O_5, to be compared to the 0.13–0.78 wt% P_2O_5 range in the PIP-RMG (Linnen and Cuney 2005). A fact to consider in this connection is the presence of mafic enclaves (MME) in the biotite granite, pointing for this type to another mingling/mixing process between a granite and a mafic magma (AKG trend in Fig. 11). The MME are microdiorite, and evidence of interaction with the hosting granite is provided (i) by the protolithionite nature of the biotites in the MME and (ii) by the presence in the granite, in the close vicinity of the enclaves, of magnesian biotite clearly derived from the MME. Despite the evidently limited extent of this interaction and owing to the lack of any phosphate in the MME, it could be suggested that the P content was diluted in the granite-biotite melt as a result of the mingling/mixing process. More likely, however, the EM1 end-member could be a highly fractionated term of an I-type suite of the Caledonian sub-type (Frost et al. 2001) (Griffel and Strontian suites in Fig. 11), and this would provide a possibly better explanation of the presence of MME in the biotite granite. Finally, the EM1 could be analogous to the peraluminous potassic Limousin type (AKL) of Stussi (1989). In the absence of trace element data for the biotite granite, it cannot be definitely concluded to the nature of the EM1 end-member.

Source of tin and tungsten for the quartz vein mineralized systems

Owing to the clear disjunction between tin and tungsten mineralization, it is likely that the two metals pertain to two different mineral systems, and therefore, the question of the metal source is indeed split into two questions. One important point is that the granites are not as much specialized as to be evident direct (magmatic-hydrothermal) source of any of the two metals.

In the case of tungsten, an interesting perspective is opened by the data on secondary rutile in both the granite and the muscovite granites. In the granite biotite, this rutile 2 is related to the muscovitization (muscovite 2) of the protolithionite. In the muscovite granite, it post-dated the muscovite 1 and could

well have also been coeval with muscovite 2. In both granite types, rutile 2 is characterized by significant tungsten enrichment. This is evidence for the presence of tungsten in the fluids associated to the muscovitization event, a fact which may be interpreted as demonstrating either that the incoming fluid was W-enriched, or to the contrary that it gained tungsten as a result of the alteration process. The second term of the alternative seems most probable, owing to the fact that the primary micas in the granites (protolithionite. Li-Fe muscovites) were likely the hosts for tungsten: indeed, no W-rich primary phase was found in the accessory mineral inventory. If so, an importance consequence is that the muscovitization process (incipient greisenization in the biotite granite) resulted in the leaching of a significant part of the total content in tungsten in the granites. It is tempting to think that this was precisely the source of the tungsten for the wolframite mineralization.

Geodynamic context

It has been recently shown that the eastern part of the Tuareg Shield was submitted to Pan-African tectono-magmatism later than the rest of the Shield, as a result of the late Ediacaran intracontinental Murzukian event (575–555 Ma), i.e., the indentation of an eastern Murzuq craton into the already structured western and central Tuareg Shield, following the older convergence (730–580 Ma) with the West African Craton (Fezaa et al. 2010; Liégeois 2019). In the central Tuareg Shield, intrusion of high-level granite plutons of the Taourirt suite was related to the simultaneous reactivation of late (transtensional) N-S megashear zones, in response to linear delamination of the SCLM (Azzouni-Sekkal et al. 2003. Liégeois et al. 2013). It has been proposed that the latest (transtensional) reactivation of the megashear zones, at 540–520 Ma (terminal Ediacaran-early Cambrian), responsible for rare metal mineralization, and inception of crustal-scale hydrothermal systems and gold mineralization, was the final manifestation, a late echo, of the Murzukian indentation process (Marignac et al. 2016). The Djanet terrane is now considered the westernmost part of the Murzuq craton (Fezaa et al. 2010; Liégeois 2019), and it is conceivable that it behaves rather rigidly (after the Ediacaran compressive deformation) at the very end of the Murzukian collision, meaning that, in the same way as for the rigid LATEA block. Late magmatism in the Djanet terrane resulted from deep crustal melting in response to linear delamination of the SCLM, possibly along deep splays of the TASZ. Thus, the differences between the late granite suites of the Djilouet group and the Taourirt/RM granites in central Tuareg Shield should be ascribed to the differences in the lithological nature of the corresponding lower crusts, rather than to the differences in the geodynamic environment.

Conclusions

- The Djilouet pluton would have been emplaced later than 558 ± 5MA and represent the latest Pan-African granite magmatism in the Djanet Terrane.
- The Djilouet magmatic trend is interpreted as a mixing process between a highly fractionated melts of the Taourirt family (central Hoggar) and a highly fractionated term of an I-type suite of the Caledonian sub-type.
- W and Sn pertain to two different mineral systems. The granites of the Djilouet cupola are not as much specialized as to be evident direct (magmatic-hydrothermal) source of any of the two metals. The metal deposition is the consequence of the granite muscovitization process (greisenization).
- The late magmatism in the Djanet terrane resulted from deep crustal melting in response to a linear delamination. Thus, the differences between the late granite suites of the Djilouet group and the Taourirt/RM granites in central Tuareg Shield should be ascribed to differences in the lithological nature of the corresponding lower crusts.

Supplementary Information The online version of this article (https://doi.org/10.1007/s12517-020-06418-z) contains supplementary material, which is available to authorized users.

Acknowledgments We are very grateful to Prof. C. Marignac for his precious aid and useful suggestions. We are indebted to the staff of the CRPG and the "Service commun de microanalyses" for their help with the analyses and to the ORGM and OPNT for the access to the workings and sites.

References

Abe T, Kuribayashi T, Nakamura M (2016) OH defects in synthetic xenotime (YPO_4). Eur J Mineral 28:641–648

Anders E, Grevesse N (1989) Abundances of the elements: meteoritic and solar. Geochimica Cosmochimica Acta 53:197–214

Atencio D, Andrade MB, Christy AG, Gieré R, Kartashov PM (2010) The pyrochlore supergroup of minerals: nomenclature. Can Mineral 48:569–594

Azzouni-Sekkal A (1995) Pétrologie et géochimie des granites de type "Taourirt": un exemple de province magmatique de transition entre les régimes orogéniques et anorogéniques au pan-africain (Hoggar. Algérie). Mémoires du Service Géologique de l'Algérie 7:1–288

Azzouni-Sekkal A, Boissonnas J (1993) Une province magmatique de transition du calco-alcalin à l'alcalin: les granitoïdes pan-africains à structure annulaire de la chaîne pharusienne du Hoggar (Algérie). Bulletin de la Société Géologique de France 164:597–608

Azzouni-Sekkal A, Liégeois JP, Bechiri-Benmerzoug F, Belaïdi-Zinet S, Bonin B (2003) The "Taourirt" magmatic province. A marker of the closing stage of the Pan-African orogeny in the Tuareg shield: review of available data and Sr-Nd isotope evidence. J Afr Earth Sci 37:331–350

Bastos Neto AC, Pereira VP, Pires AC, Barbanson L, Chauvet A (2012) Fluorine-rich xenotime from the Nb–ta–Sn Madeira world-class deposit associated with the albite-enriched granite at Pitinga. Amazonia. Brazil. Can Mineral 50:1019–1032

Bau M (1996) Controls on the fractionation of isovalent trace elements in magmatic and aqueous systems: evidence from Y/Ho. Zr/Hf and lanthanide tetrad effect Contributions to Mineralogy and Petrology 123:323–333

Bechiri-Benmerzoug F, Bonin B, Bechiri H, Khéloui R, Talmat-Bouzeguela S, Bouzid K (2017) Hoggar geochronology: a historical review of published isotopic data. Arab J Geosci 10:351–383

Bouabsa L (1987) Intrusions granitiques à albite-topaze: minéralisations stanno-wolframifères et altérations hydrothermales associées. L'exemple du Hoggar central. Algérie. Thèse de 3ème cycle. Université Nancy I. 193p

Cerny P. Blevin PL. Cuney M. London D (2005) Granite-related ore deposits. Economic Geology 100th Anniversary Volume: 337–370

Chalal Y. Marignac C (1997) Découverte de wolframoixiolite dans les microgranites à albite-topaze d'Aleméda (Hoggar central. Algérie): implications métallogéniques. Bulletin Service Carte Géologique Algérie 8. 1. 71–79

Cheilletz A, Bertrand JM, Charoy B, Moulahoum O, Bouabsa L, Farrar E, Zimmermann JL, Dautel D, Archibald DA, Boulier AM (1992) Géochimie et géochronologie Rb-Sr. K-Ar et 40Ar/39Ar des complexes granitiques pan-africains de la région de Tamanrasset (Algérie): relations avec les minéralisations Sn - W associées et l'évolution tectonique du Hoggar central. Bulletin Société Géologique France 163(6):733–750

De La Roche H, Stussi JM, Chauris L (1980) Les granites à deux micas hercyniens français. Essais de cartographie et de corrélations géochimiques appuyés sur une banque de données, implications pétrologiques et métallogéniques. Sciences de la Terre, XXIV 1:5–121

Debon F, LeFort P (1988) A chemical-mineralogical classification of common plutonic rocks and associations. Trans Roy Soc Edinburgh, Earth Sci. 73:135–149

El-Bouseily AM, El-Sokkary AA (1975) The relation between Rb. Ba. and Sr in granitic rocks. Chem Geol 16:207–219

European Commission (2017) Communication from the Commission to the European Parliament. The Council. the European Economic and Social Committee and the Committee of the Regions on the 2017 list of Critical Raw Materials for the EU. 7 pp.

Fezaa N (2010) Géochronologie et géochimie du magmatisme panafricain de Djanet et de son encaissant métasédimentaire (Hoggar oriental. Algérie). Conséquences Géodynamiques. Thèse doctorat. USTHB. Alger. 254p

Fezaa N, Ouabadi A, Liégeois JP, Abdellah N, Waele B, Bruguier O (2006) Le terrane de Djanet: Géochronologie et géochimie de ses sédiments ; lien avec le métacraton Saharien. *4th I. G. C. P 485 p 43*

Fezaa N, Liégeois JP, Abdallah N, Cherfouhd EH, Waele B, Bruguier O, Ouabadi A (2010) Late Ediacaran geological evolution (575–555 Ma) of the Djanet Terrane. Eastern Hoggar. Algeria. Evidence for a Murzukian intracontinental episode. Precambrian Res 180:299–327

Fezaa N, Liégeois JP, Abdallah N, Bruguier O, Laouar O, Ouabadi A (2013) Origine du groupe métasédimentaire de Djanet (Hoggar oriental. Algérie). géochronologie et géochimie. Bulletin du Service Géologique National de l'Algérie 24:3–26

Fowlers MB, Kocks H, Darbyshire DPF, Greenwood PB (2008) Petrogenesis of high Ba-Sr plutons from the northern highlands terrane of the British Caledonian Province. Lithos 105:129–148

Frost BR, Barnes CG, Collins WJ, Arculus RJ, Ellis DJ, Frost CD (2001) A geochemical classification for granitic rocks. J Petrol 42:2033–2048

Hughes CJ, Hussey EM (1976) M and Mg values in igneous rocks: proposed usage and a comment on currently employed Fe_2O_3 corrections. Geochimica Cosmochimica Acta 40:485–486

Irber W (1999) The lanthanide tetrad effect and its correlation with K/Rb. Eu/Eu*. Y/Ho and Zr/Hf of evolving peraluminous granite suites. Geochimica Cosmochimica Acta 63. Mineralogist 80:94–108

Kesraoui M (1990) Greisenisation et minéralisations W-Sn à Tin-Amzi (Hoggar central). Typomorphisme des minéraux et aspects géochimiques. Thèse de Magister. IST/USTHB, Alger, 180 p

Kesraoui M, Nedjari S (2002) Contrasting evolution of low-P rare metal granites from two different terranes in the Hoggar area. Algeria. J Afr Earth Sci 34:247–257

Kesraoui M, Marignac C, Verkaeren J (2000) L'évolution tardimagmatique des granites à métaux rares: l'exemple de la coupole de Tin-Amzi (Hoggar-Algérie). Bulletin Service Géologique Algérie 11(2):195–216

La Roche (de) H, Stussi JM Chauris L (1980) Les granites à deux micas hercyniens français. Essais de cartographie et de corrélations géochimiques appuyés sur une banque de données, implications pétrologiques et métallogéniques. Sciences de la Terre, XXIV 1:5–121

Lamri T, Djemaï S, Hamoudi M, Zoheir B, Bendaoud A, Ouzegane K, Amara M (2016) Satellite imagery and airborne geophysics for geologic mapping of the Edembo area. Eastern Hoggar (Algerian Sahara). J Afr Earth Sci 115:143–158

Liégeois JP (2019) A new synthetic geological map of the Tuareg shield: an overview of its global structure and geological evolution. Springer Nature Switzerland AG 2019. In: Bendaouad et al (eds) The Geology of the Arab World- An Overview. Springer Geology, pp 83–107. https://doi.org/10.1007/978-3-319-96794-3-2

Liégeois JP, Latouche L, Boughrara M, Navez J, Guiraud M (2003) The LATEA metacraton (Central Hoggar. Tuareg Shield. Algeria): behaviour of an old passive margin during the Pan-African orogeny. J Afr Earth Sci 37:161–190

Liégeois JP, Benhallou A, Azzouni-Sekkal A, Yahiaoui R, Bonin B (2005) The Hoggar swell and volcanism: reactivation of the Precambrian Tuareg shield during Alpine convergence and West African Cenozoic volcanism. Geol Soc Am Spec Pap 388:379–400

Liégeois JP, Abbelsalam MG, Ennih N, Ouabadi A (2013) Metacraton: nature. Genesis and behavior. Gondwana Res 23:220–237

Lin Y, Pollard PJ, Hu S, Taylor RG (1995) Geologic and geochemical characteristics of the Yichun Ta-Nb-Li deposit. Jiangxi Province. South China. Econ Geol 90:577–585

Linnen RL, Cuney M (2005) Granite-related rare-element deposits and experimental constraints on Ta-Nb-W-Sn-Zr-Hf mineralization. In: Linnen. R.L.. and Samson. I.M.. eds.. Rare-element geochemistry and mineral deposits: geological association of Canada. GAC Short Course Notes 17:45–68

Maniar PD, Piccoli PM (1989) Tectonic discrimination of granitoids. Geol Soc Am Bull 101:635–643

Marignac C, Aïssa DE, Bouabsa L, Kesraoui M, Nedjari S (2016) The Hoggar gold and rare metals metallogenic province of the Pan-African Tuareg Sheild (Central Sahara. South Algeria): an early Cambrian Echo of the late Ediacaran Murzukian avent? In: Bouabdellah A, Slack JF (eds) Mineral deposits of North Africa. Mineral resource Rewiews. Springer International Publishing Switzerland, pp 371–404. https://doi.org/10.1007/978-3-319-31733-5-15

Mesbah A, Clavier N, Lozano-Rodriguez J, Szenknect S, Dacheux N (2016) Incorporation of thorium in the zircon structure type through the $Th_{1-x}Y_x(SiO_4)_{1-x}(PO_4)_x$ thorite-xenotime solid solution. Inorg Chem 55:11273–11282

Monecke T, Kempe U, Sala M, Wolf D (2002) Tetrad effect in rare earth element distribution patterns: a method of quantification with application to rock and mineral samples from granite-related rare metal deposits. Geochimica Cosmochimica Acta 66:1185–1196

Monier G, Robert J-L (1986a) Muscovite solid solutions in the system K_2O-MgO-FeO-Al_2O_3-SiO_2-H_2O: an experimental study at 2 kbar PH_2O and comparison with natural Li-free white micas. Mineral Mag 50:257–266

Monier G, Robert J-L (1986b) Evolution of the miscibility gap between muscovite and biotite solid solutions with increasing lithium content: an experimental study in the system K_2O-Li_2O-MgO-FeO-Al_2O_3-SiO_2-H_2O-HF at 600°C. 2 kbar PH_2O: comparison with natural lithium micas. Mineral Mag 50:641–651

Nedjari S, Kesraoui M, Marignac C, Aïssa DE (2001) Le massif d'Ebelekan: un granite _a tantale dans le Sud-Est du Hoggar Central (Algérie). Bulletin Service Géologique Algérie 12:15–47

Nemmour-Zekiri D (2012) Evolution thermo-mécanique et tectono-sédimentaire du bloc de Djanet (Hoggar Oriental. Algérie). Thèse doctorat d'état. USTHB. Alger. 116p

Nemmour-Zekiri D. Mahdjoub Y (2012) Déformations panafricaines et post-panafricaines dans la région de Djanet. (Hoggar oriental. Algérie). Bulletin Service Géologique National vol. 23. n°2. pp. 117–135

Nemmour-Zekiri D, Oulebsir F, Mahdjoub Y, Kesraoui M (2006) Eléments de géologie de la région de Djanet (Hoggar oriental. Algérie). In: The 3rd Conf. Ass. Afr. Women. Geoscie. Marco Univ, pp 166–167

Oulebsir F (2009) Pétrographie. géochimie et minéralisations à Sn-W associées du massif de Djilouet (Djanet. Hoggar Oriental). Mémoire de Magister. USTHB. Alger. 110 p

Oulebsir F, Kesraoui M (2006) Etude préliminaire des minéralisations à W - Sn associées à la coupole granitique de Djilouet (Djanet. Hoggar Oriental). XIIème Sém. N. S.T. Oran. pp. 67–68

Oulebsir F, Kesraoui M, Nemmour-Zekiri D (2013) Les minéralisations associées aux de la région de Tamrirt. Djanet Hoggar Oriental. Algérie. 8ème Colloque International. Magmatisme. Métamorphisme et Minéralisations Associées. Marrakech. Maroc, p 221

Raimbault L, Cuney M, Azencott C, Duthou JL, Joron JL (1995) Geochemical evidence for a multistage magmatic genesis of Ta-Sn-Li mineralization in the granite at Beauvoir. French massif central. Econ Geol 90:548–576

Rougier S (2012) Interactions lithosphère – asthénosphère et mouvements verticaux: le cas du massif du Hoggar. PhD. Université Paris Sud - Paris XI. https://tel.archives-ouvertes.fr/tel-00788392

Rudnick RL, Gao S (2003) Composition of the continental crust. In: Holland HD. In: Turekian KK (ed) Treatise on Geochemistry. Elsevier (2005). Chapter 3. The crust, pp 1–56

Sasaki A (1959) Variation of unit cell parameters in wolframite series. Min J 2:375–396

Soéda A, Takeno S, Watanabe M (1979) Mineralogical study on the wolframite series from the chugoku district. Southwest Japan (I). Relationships between lattice parameters and chemical compositions. J Japan Assoc Miner Petr Econ Geol 74:357–375

SONAREM report (1986) Rapport sur les résultats de la recherche détaillée et de la prospection – estimation du gisement d'étain et de wolframite de Djilouet effectuées de 1982–1986. Unpublished report

Soufi M (1988) Etude des magmatismes leucogranitique et ongonitique de Blond (Haut Limousin Massif Central français). Relations avec une mise en place syntectonique du massif granitique. Unpubl. phD Thesis. Nancy I University. 304 pp

Stussi J-M (1989) Granitoid chemistry and associated mineralization in the French Variscan. Econ Geol 84:1363–1381

Talla D, Beran A, ŠkoDa R, Losos Z (2011) On the presence of OH defects in the zircon-type phosphate mineral xenotime. (Y.REE)PO_4. Am Mineral 96:1799–1808

Teng FZ, McDonough WF, Rudnick RL, Dalpé C, Tomascak PB, Chappell BW, Gao S (2004) Lithium isotopic composition and concentration of the upper continental crust. Geochimica Cosmochimica Acta 68:4167–4178

Tischendorf G, Förster H-J, Gottesmann B (1999) The correlation between lithium and magnesium in trioctahedral micas: Improved equations for Li_2O estimation from MgO data. Mineralogical Magazine 63(1):57–74

Uher P, Ondrejka M, Broska I (2007) S and As in accessory monazite: a role of "clinoanhydrite" and gasparite substitution. EGU 2007. Geophysical Research Abstracts 9:09146

Whitney DL, Evans BW (2010) Abbreviations for names of rock-forming minerals. Am Mineral 95:185–187